Thin Film Gas Sensors Based on Zinc Oxide Nanoinks

By
Pengjun Duan

A Project Report Submitted in Partial Fulfillment of the
Requirements for the Degree of

MASTER OF ENGINEERING

in the Department of Electrical & Computer Engineering

Supervisory Committee

Thin Film Gas Sensors Based on Zinc Oxide Nanoinks

By

Pengjun Duan

Bachelor of Science, The Pennsylvania State University, 2016

Supervisory Committee

Dr. Christo Papadopoulos, Supervisor
Department of Electrical & Computer Engineering

Dr. Mihai Sima, Departmental Member
Department of Electrical & Computer Engineering

Abstract

Planetary ball milling (PBM) is a high-energy ball milling technology that was used in this study to fabricate zinc oxide (ZnO) nanoinks via nano grinding, followed by the fabrication of thin film chemiresistive gas sensors via the doctor blading method, which operated at room temperature. In order to create the different thin film gas sensor samples (with different particle sizes and porosity), the ZnO nanoinks were prepared by changing the grinding parameters, such as grinding time, grinding speed and solvents (ethylene glycol (EG) and deionized (DI) water). To study the gas sensing performance, we tested these gas sensor device samples using dry air/oxygen against hydrogen, argon and methane target gases, in addition to different temperatures and relative humidity, under ambient light conditions. In this report, the particle size and RMS film roughness were measured by atomic force and scanning electron microscopy; the purity and structure of ZnO nanoparticles are confirmed by Raman spectroscopy, photoluminescence, and x-ray analysis. At room temperature, the gas sensor response of thin film samples reached a peak for nanoinks milled at 400 rpm and 30 min. This can be related to the increase of film porosity and the enhancement of electron concentration change, caused by oxygen ion adsorption/desorption on the surface of zinc oxide nanoparticles. In addition, research also indicated that the sensor response and dynamic behaviour improves with increasing temperature, reaching a maximum value between 100 – 150 ºC. Our study demonstrates the application of low-cost PBM nanoink as an active material for solution processed thin film gas/humidity sensors, and provides some suggestions to improve gas sensors in future study, such as measuring system, ZnO nanomaterials with different morphologies, and doping.

Table of Contents

List of Tables

List of Figures

List of Acronyms

PBM - Planetary Ball Milling

LOD – Limit of Detection

RMS - Root-mean-square

SMO - Semiconductor Metal Oxide

AFM - Atomic Force Microscopy

SEM - Scanning Electron Microscope

FESEM - Field Emission Scanning Electron Microscopy

Acknowledgements

I would like to thank my supervisor Dr. Chris for his guidance throughout my degree, and for being a reliable source of motivation, knowledge, and wisdom.

I would also like to express gratitude towards my colleagues and friends, especially Raju, whose help and moral support were invaluable.

Finally, I'd like to thank my family for their generous support and patience which has enabled me every opportunity. In addition, I wanted to thank the patience, care and support from Shimeng Zhang over the past years.

Chapter 1

Introduction

1.1 Motivation

The development of nanotechnology promotes the integration of many disciplines and different research fields. As a new field of materials science, functional materials of nanostructures have been the focus of research in the world in recent decades [1]. However, the complex fabrication process and high cost of products have been bothering many scientists, even limiting their application in practical production [2]. Therefore, the low cost of raw materials, the universality and controllability of technology, the controllability of material form, and environmental protection have gradually become the goal that human beings are constantly perusing. The ball milling technique is a simple, economical, high-yield and practical method, which has been gradually recognized and expected to solve the problem of mass production of nanomaterials [3].

1.1.1 Nanomaterials

Nanomaterials refer to any material with crystal, amorphous, quasicrystal and interface layer structures that have dimensions in the range is 0.1-100nm [4]. Particle size reduction to one nanometer will present surface and interface effect, quantum size effect, small size effect and macro quantum channel effect [5]. These effects make nanomaterials have many unique properties. The basic units of nanomaterials can be divided into three categories according to their spatial dimensions [6]: (1) zero dimensional nanomaterials, which are all in the nanoscale in three-

dimensional space, such as nanoparticles and atomic clusters; (2) one dimensional nanomaterials, which are in two-dimensional space, such as nanowires and nanorods; (3) two-dimensional nanomaterials, in three-dimensional space, which are one dimension in nanoscale, such as ultrathin film, multilayer film, superlattice and etc [2]. Due to these units often having quantum properties, the zero dimensional, one dimensional and two-dimensional basic units are called quantum dots, quantum wires and quantum well respectively.

With the unique optical, electrical, magnetic, and catalytic properties of the Nanomaterials, it can be widely used in many fields, which involved national defense and military applications, such as nano robots, uniforms [7], and civil industry, such as chemical sensors, nano transistors, OLED, quantum computer, etc. [8] Especially for transistors, by applying Moore's law [9, 10], the amount of transistors and resistors in a chip getting doubles every single year. By shrinking the size of transistors, the performance and capacity of semiconductors will exponentially strengthen. As shown in Figure 1.1 [11], the number of transistors is increased at an exponential rate. Thus, Nanomaterials is not only playing an irreplaceable role in the high-tech industry but also provide significant opportunities and innovative ideas to the traditional industries. With the continuous development of nanomaterial preparation technologies and the expansion of its application fields, the industrial production of nanomaterials will have a significant impact on the traditional chemical industry and other industries.

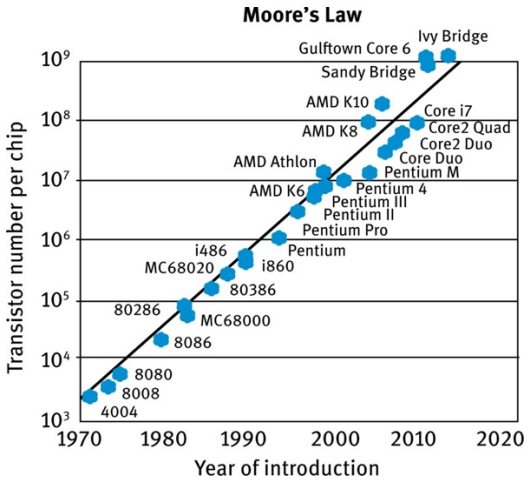

Figure 1.1 Trends in CPU processor transistor count data. [11]

1.1.2 Gas Sensor

In recent decades, with the rapid development of industrialization and urbanization, air pollution has become the main concern of many countries. Clean air is essential to our health and environment. The serious air pollution (mainly caused by factory emission and automobile exhaust) has become a great threat to human survival and development. Atmospheric pollution caused by a large number of trace gases (such as nitrogen oxide, sulfur dioxide, carbon dioxide, carbon monoxide, methane etc. [12]) intensifies the greenhouse effect, and causes problems such as acid rain, photochemical smog and global climate change. At the same time, the detection and monitoring of combustible gas (such as hydrogen, methane, ethanol and carbon monoxide) [13, 14], toxic gas (such as nitrogen dioxide and ammonia) [15] and exhaust gas (nitrogen dioxide and sulfur dioxide) [16] are also very important for energy saving and environmental protection. This is especially true for methane as the main component of natural gas, which is closely related to people's daily activities and life [17]. As well as for hydrogen gas (H_2), as a clean energy source, which has attracted extensive attention in recent years. However, due to its flammable concentration in the air of 4 vol.%, there are potential safety hazards during use, transportation and

storage. If leakage occurs, it may cause casualties and property damage [18]. Therefore, it is urgent to use gas sensors to detect these harmful gases in real time and effectively. Gas sensors can convert the required chemical reactions into measurable electronic signals, such as changes in resistance, frequency, current or voltage. The performance of gas sensors needs to be evaluated by various parameters, which including sensitivity, selectivity, accuracy, limit of detection (LOD), resolution, accuracy, reversibility, recovery time and response time. Gas sensors with its low cost, reliability, small volume, low power consumption and long life, are the key factors for the realization of gas sensors in various applications [5]. With the increasing demand for better gas sensors (higher selectivity and sensitivity), human is trying to find more suitable materials with required surface and bulk properties. Among many semiconductor gas sensors, the semiconductor metal oxide (SMO) gas sensor is the most studied one. It has been widely studied for its high gas response, excellent selectivity, good portability, and low manufacturing cost. Recently, nano semiconductor metal oxides (with sizes ranging from 1 nm to 100 nm) are increasingly used for gas sensing due to their size dependence[19]. Nanomaterials have unique mechanical, optical, electrical, catalytic, and magnetic properties. In addition, these materials also have higher specific surface area per unit mass and new physical and chemical properties. With the decrease of material size, the specific surface area and specific surface area increase sharply. Moreover, the motion of electrons and holes in semiconductor nanomaterials is also affected by the size and geometry of the materials. Therefore, there are various crystal structures, noble metal doping ability, and better sensitivity that fulfills the production for demand of gas sensors nanoparticles. [18]

1.2 Background

1.2.1 Method of Fabrication: Ball Milling

Ball milling is also called mechanical ball milling or high-energy mechanical ball milling. It mainly uses the extrusion force and shear force between grinding media to crush materials in a ball mill. The main process is to put the powder with different composition into the ball milling tank and mill it on the ball mill for a long time [20]. In the process of ball milling, the mechanical energy of the ball milling medium is transferred to the powder in different forms by the violent collision, extrusion and friction between the ball milling medium and the ball milling medium, and between the powder and the wall of the ball milling tank [16]. In general, in the planetary ball milling, the rotation direction of pots and the disks are in opposite directions (as shown in Figure 1.2) [21]. In the process of ball milling, the powder is trapped in frequent collisions, resulting in strong plastic deformation, repeated crushing smoke in one crushing process, and its microstructure is constantly refined, which makes the large grains become small grains. Ball milling can synthesize high friction point metals, alloys and composites which are difficult to obtain by conventional methods, and it has been widely studied because of its simple process, low cost, and high efficiency [22]. It can obtain kilogram products at one time and is suitable for industrial production. After decades of development, the ball milling method has been extended and expanded. In addition to the direct preparation of nanocrystals and nanocomposites by ball milling technology, one-dimensional or two-dimensional nanomaterials are often prepared by ball milling powder through high-temperature heat treatment or chemical treatment. Therefore, all methods including the ball milling process can be collectively referred to as ball milling method.

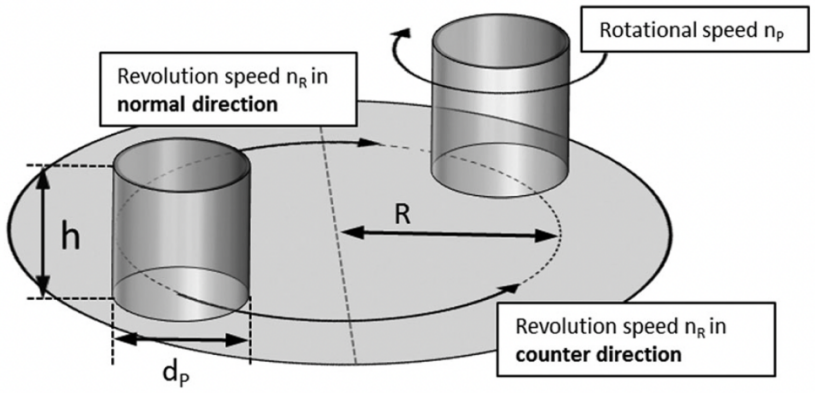

Figure 1.2 Scheme of planetary disks with movement in a normal and counter direction; with pot height h; pot diameter d_P; revolution radius R. [21]

Scientific experiments and theoretical research show that the rotation speed of a mill barrel has a great influence on the grinding effect of the grinding medium. As same mill is rotated at different speeds, there are three different states of grinding media. While the rotation speed is very low, all height of media is small, and it only deflects upward for a certain angle, in this instance, each medium rotates around its own axis [23]. As the rotation speed is too low, the friction force of the lining plate on the medium is not enough to bring them to a certain height. When the grinding medium reaches its natural angle of repose, the medium rolls down the slope. This movement is called the box down state. When the mill works in the state of falling at night, the material is mainly subjected to grinding and stripping between the media, and the impact kinetic energy is small, so the crushing efficiency is not high [24]. When the rotational speed of the mill is too high, the ball milling media will produce a great centrifugal inertia force, which makes them stick to the inner surface of the mill cylinder liner and make a constant velocity circular motion with it. In this case, there is no impact on the medium, the grinding and stripping effect is very weak, and the grinding effect almost stops, which is called the centrifugal state. When the mill speed is moderate, the lifting friction of the liner gives the ball milling a certain height, so the ball milling medium

has a large impact on kinetic energy. This state is called the explosive cloth state or dropping state. In the mill in the dropping state, the material is subjected to the grinding and stripping action of the medium in the circular curve movement area. In the place where the medium falls, the material is subjected to the impact of the medium and the strong rolling, grinding, and stripping action, so the crushing efficiency in this state is higher [24].

At present, ball milling has been widely used in the preparation of ultra-fine powder and nano powder, nano composite materials, dispersion strengthened alloy structural materials, metal refining, mineral and waste treatment, synthesis of new materials, and has shown unique advantages. Ball milling is widely used in the preparation of nanoparticles, nanocomposites, high temperature compounds, dispersion strengthened structural materials, metal refining, mineral and waste treatment, polymer modification and synthesis of new materials [25].

1.2.2 Material overview: Zinc oxide

Zinc oxide is an important multifunctional n-type semiconductor oxide material, which belongs to the II-VI semiconductor. Although zinc oxide exists naturally in the form of zinc ore, but most of them are synthetic in lab research, due to its impurities. Zinc oxide is a white powder, insoluble in water, soluble in acid and strong base. As a common chemical additive, zinc oxide is widely used in the production of plastics, silicate products, synthetic rubber, lubricants, coatings, ointments, adhesives, food, batteries, flame retardants and etc. ZnO has a large bandgap and exciton binding energy, high transparency, and excellent room temperature luminescence properties. At room temperature, the direct bandgap is about 3.37 eV, and the exciton binding energy is 60 meV [5]. Compared with other semiconductor materials, it has the advantages of fast

response, short response/recovery time, good electrical properties, and long-term stability. It is widely used in active gas sensing materials, liquid crystal displays, thin film transistors, light-emitting diodes, and other products in the semiconductor field.

Molar mass	Density	Melting point	Boiling point
81.406 g/mol	5.606 g/cm^3	1,974 °C	1,974 °C
Bandgap	Exciton energy	Electron mobility	Hole mobility
3.3 eV	60meV	2000 cm2V-1s-1 (80K)	5-30 cm2V-1s-1

Table 1.1: Material properties of zinc oxide [26, 27]

Crystal structure and lattice parameters

Zinc oxide is a typical II-VI semiconductor compound. It can be divided into two crystal structures (Fig. 1.3): hexagonal wurtzite structure and cubic sphalerite structure [28]. Under ambient pressure and temperature, ZnO crystallizes in wurtzite (B4 type) structure, which is a hexagonal lattice belonging to space group P6$_3$*mc*. It is characterized by two interconnected sublattices Zn^{2+} and O^{2-}, so that each zinc ion is surrounded by a tetrahedral oxygen ion. This tetrahedral coordination produces polar symmetry along the hexagonal axis. This polarity determines many characteristics of ZnO, including its piezoelectric and spontaneous polarization. It is also a key factor for crystal growth, etching and defect generation. In addition to causing the inherent polarity in ZnO crystals, the tetrahedral coordination of the compound is also a common

indicator of sp^3 covalent bond. However, the Zn–O bond also has very strong ionic properties, so ZnO at the boundary between covalent compounds and ionic compounds, with the ionic degree f_i = 0.616 [29]. The lattice parameters of hexagonal cells are a = 3.2495 Å and C = 5.2069 Å, and the density is 5.605 gcm^{-3}. In an ideal wurtzite crystal, the axial ratio c/a and u parameters (a measure of the displacement of each atom relative to the next atom along the c-axis) are related by the relationship $uc/a = (3/8)^{1/2}$, where $c/a = (8/3)^{1/2}$ and u =3/8 represent an ideal crystal. By changing these two values, ZnO crystals deviate from this ideal arrangement. This deviation makes the tetrahedral distance roughly unchanged in the lattice. Experimentally, for wurtzite zinc oxide, the actual values of u and c/a are determined in the range of u = 0.3817–0.3856 and c/a = 1.593 – 1.6035 which is close to the ideal value of hexagonal cell c/a = 1.633 [30].

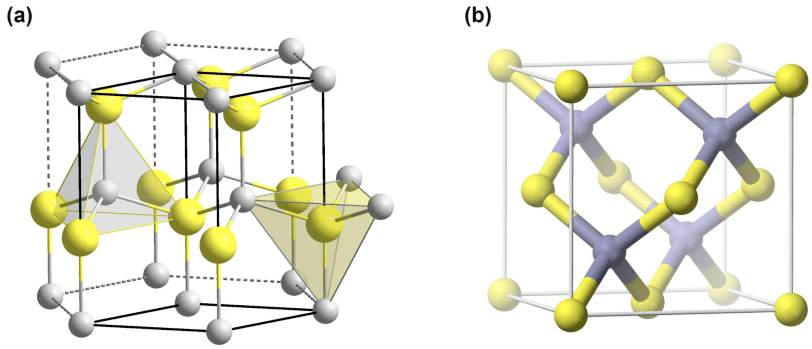

Figure 1.3 The main crystal structures of ZnO. (a) hexagonal wurtzite (b) cubic zinc-blende [28].

Energy bandgap

Lots of groups have calculated the electronic band structure of ZnO. Figure 1.4 [30] shows the calculation results of accurately explaining the band structure of Zn 3D electrons using local density approximation (LDA) combined with atomic self-interaction correction pseudopotential

(SIC-PP). In the hexagonal brillouin region, the energy band structure is displayed along the high symmetry line. The maximum value of valence band and the minimum value of lowest conduction band appear at k = 0 indicates that ZnO is a direct bandgap semiconductor. The conduction band of ZnO is mainly s-like, while the valence band is p-like. The bandgap determined from this calculation is 3.77 eV. This has a good correlation with the experimental value of 3.4 eV and is closer to the value calculated by the standard LDA. Experimentally, the valence band of ZnO is divided into three band states A, B and C by spin-orbit and crystal field splitting. The split is shown in Figure 1.5 [30].

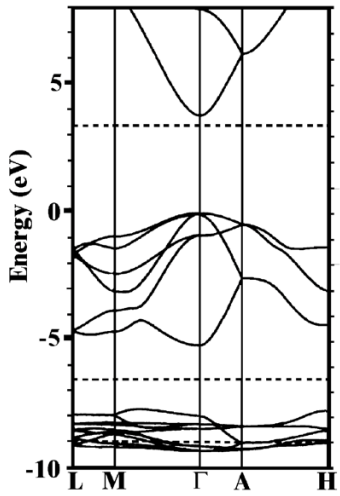

Figure 1.4 The LDA band structure of bulk wurtzite ZnO calculated using dominant atomic self-interaction-corrected pseudopotentials (SIC-PP). This method is much more efficient at treating the d-bands than the standard LDA method. [30]

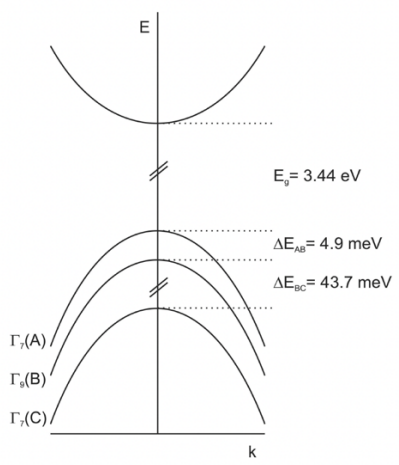

Figure 1.5 Schematic diagram representing the crystal-field and spin-orbit splitting of the valence band of ZnO into 3 subband states A, B and C at 4.2 K. [30]

Electronic and Optical Properties

There are many controversial issues about the optical and electronic properties of ZnO, such as green emission and p-type doping. Due to the great difference in the quality of available samples, the electrical properties of ZnO are difficult to quantify. The background carrier concentration varies greatly according to the mass of the layer, but it is usually $\sim 10^{16} cm^{-3}$. It is reported that the largest n-type doping is $\sim 10^{20}$ electron cm^{-3} and the largest p-type doping is $\sim 10^{19}$ hole cm^{-3}. At 300K, the exciton binding energy is 60 meV, which is one of the reasons why ZnO is attractive in optoelectronic devices. The electron effective mass is $0.24m_0$ and the hole effective mass is $0.59m_0$. For low n-type conductivity, the corresponding electron hall mobility at 300K is μ= 200 $cm^2V^{-1}s^{-1}$, 5 – 50 $cm^2V^{-1}s^{-1}$ for low p-type conductivity [30]. The optical properties of ZnO are seriously affected by band structure and lattice dynamics. The wide peak associated with defects ranging from ~ 1.9 to ~ 2.8 eV is also a common optical feature of ZnO. Known as

the green band, the origin of its luminescence is still not well understood and has been attributed to various impurities and defects in the past. As shown in Fig. 1.6 [31], different defects may lead to energy levels in the ZnO gap.

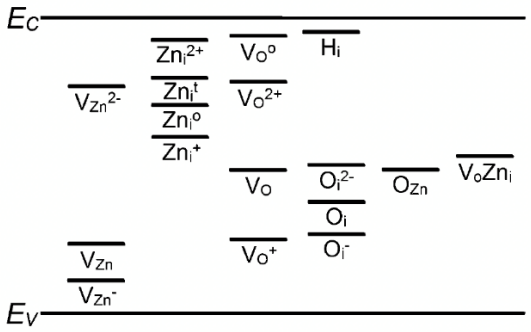

Figure 1.6 Calculated energy levels of different defects in ZnO. All the levels are referred to the conduction-band minimum (CBM). V_{ZN}, V^{-}_{Zn} and V^{2-}_{Zn} represent neutral, single charge and double charge zinc vacancies, respectively. Zn^{o}_{i} and Zn^{t}_{i} represent neutral octahedral zinc gap and neutral tetrahedral zinc gap, while Zn^{+}_{i} and Zn^{2+}_{i} represent single charge and double charge zinc gap. V^{0}_{o} and V_{o} represent neutral oxygen vacancies, while V^{+}_{o} and V^{2+}_{o} represents single charge and double charge oxygen vacancies. H_i and O_i represent oxygen and hydrogen gaps, O_{Zn} represents anti position oxygen, and V_oZn_i represents the complex of oxygen vacancy and zinc gap, respectively. [31]

Being a part of nanomaterial, ZnO nanoparticles begin to play a role in related fields. ZnO nanomaterials are ZnO nanoparticles with a diameter less than 100 nm. They have a large specific surface area and high catalytic activity. The exact physical and chemical properties of ZnO nanoparticles depend on different synthesis methods. In fact, ZnO nanomaterials have the most abundant morphology so far. For example, ZnO quantum dots with zero dimensional ZnO

nanostructures, one-dimensional ZnO nanorods, nanowires, nanotubes and nanobelts, two-dimensional ZnO nanofilms, three-dimensional ZnO nanonests, nanosprings, nanorings, nanobows and tetragonal whiskers, etc. Fig. 1.7 shows ZnO nanomaterials with different sizes [32]. It has many special properties, such as non-migration, fluorescence, piezoelectricity, absorption and scattering of ultraviolet light, etc. With excellent optical, electrical, magnetic and sensitivity, it can be used to manufacture gas sensors, phosphors, varistors, UV shielding materials, image recording materials, piezoelectric materials, varistors and high-performance materials, high-efficiency catalysts, magnetic materials, and films, etc. [26, 33-35]

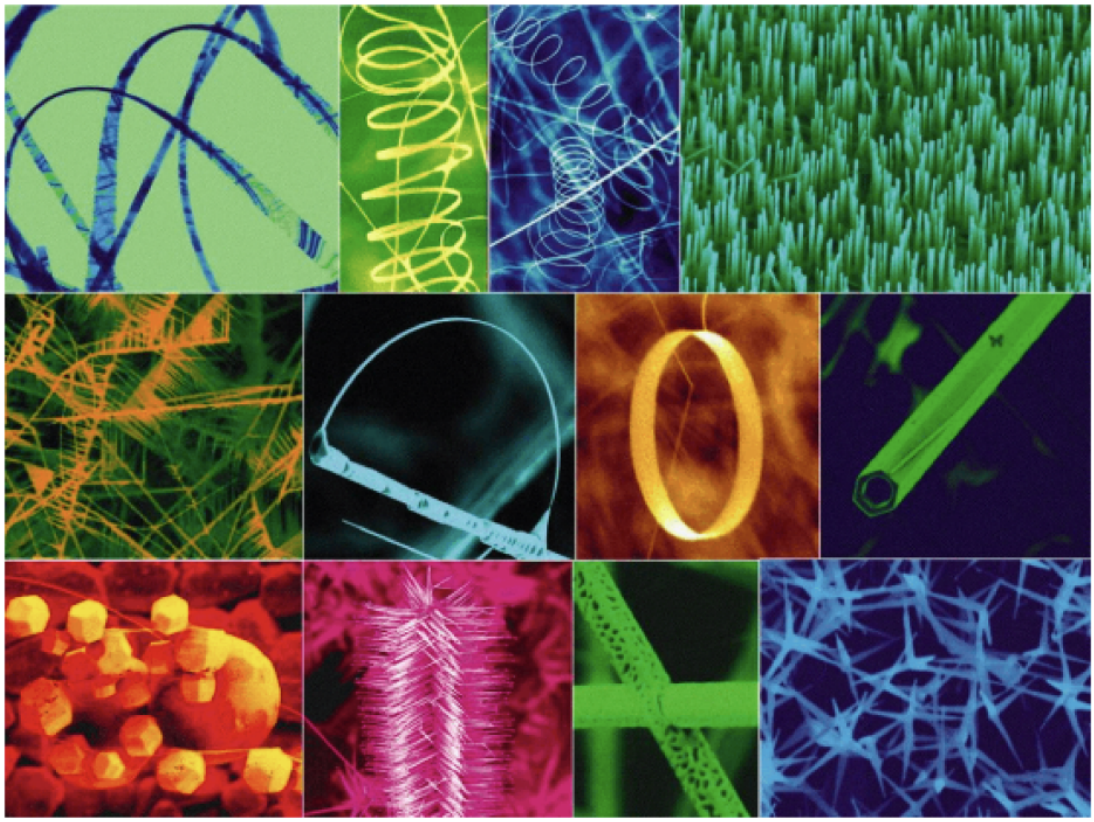

Figure 1.7 Various ZnO nanostructured synthesized by thermal evaporation under controlled conditions.[32]

1.2.3 Application of ZnO nanomaterials

Electronics and Optoelectronics Applications

Zinc oxide (ZnO) has drawn extensive attention and fieldwork in the field of electronics and optoelectronics and research, due to its bargain and excellent properties attributes, it is widely used as transparent conductive oxide (TCO) and thin film transistors (TFTs) [36]. The growing demand for TCO, which has been used as an electrode for optical and electronic devices, such as displays, solar cells, LEDs, and OLEDs [37]. At present, although indium tin oxide (ITO) has been applied as TCO in commercial products since it has excellent transparency and conductivities. However, due to the high- cost and availability limitation [38], in recent years, ZnO has been applied as an alternative TCO material with its excellent properties. With satisfactory transparency and conductivity, ZnO is already used widely at fair prices. Transparent ZnO thin films have great conductivity with high crystallinity and are straightforward to process at a low cost. Agura et al. [39] have reported resistivity was 8.1×10^{-5} Ω cm for Al-doped ZnO (AZO) thin film, which the transparency is 90% equivalent greater than ITO [40].

According to the size of band gap, semiconductor materials can be divided into narrow band gap materials and wide band gap materials. They can also be divided into indirect band gap materials and direct band gap materials. Narrow band gap materials with direct band gap are suitable for optoelectronic devices in visible/infrared region, while wide band gap materials with direct band gap are suitable for optoelectronic devices in UV/blue region [29]. Optoelectronic devices in the range of UV/blue spectrum have great demand in commercial applications such as astronomy, medical treatment, health care, water treatment, military etc. The development of blue LED has led to the development of low-power white LED, which is replacing incandescent lamp

and fluorescent lamp. Blue LEDs have also led to the development of Blu ray disks for storing high-definition video. Therefore, wide band gap semiconductors such as GaN and ZnO have attracted considerable attention. The large band gap and high exciton energy of ZnO make it an ideal material for blue and UV LEDs (Figure 1.8 shows the device structure of the ZnO pn-homojunction LED [41]). [42]. The exciton binding energy of ZnO at room temperature is 60 meV and that of GaN is 25 meV, which makes ZnO an effective emitter in the UV spectral region [29]. Therefore, the research interest in ZnO is growing greatly. Because of ZnO is widely available and cheap, so it has more advantages than GaN in terms of cost. The limiting factor of realizing ZnO based LED is the lack of stable and reproducible p-type ZnO. The alternative method is that n-type ZnO films are grown on other p-type materials, such as Si, GaN, ZnTe, Cu_2O, GaAs, etc [29]. Rogers et al. [43] have reported that n-ZnO/p-GaN LED in UV and found the peak at 375nm which fabricated using pulsed laser deposition process.

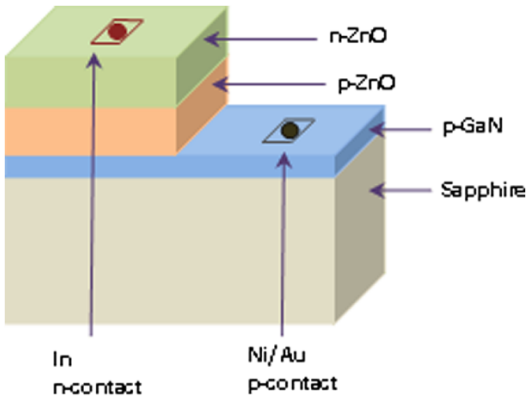

Figure 1.8 Device structure a homojunction ZnO LED making use of a p-GaN hole injection layer. [41]

Gas Sensor

With the development of modern industry, a growing number of toxic and harmful gases produced in people's production activities, especially the flammable and explosive gases, which produced in the chemical production process. It poses a great threat to the safety of people's lives and property, and the monitoring of gas sensors in the production process is becoming increasingly important [44]. In order to achieve high sensitivity and response value, ZnO based gas sensors often need high working temperature to improve their surface redox reaction rate [45], which greatly limits the application range of ZnO gas sensor in the monitoring of flammable and explosive gases, and greatly reduces its safety. At the same time, high working temperature also means large energy consumption and shortened service life, as well as the increase of equipment production and maintenance costs. Therefore, it is an important and challenging task to reduce the working temperature of the ZnO gas sensor and improve the sensing performance at room temperature.

The synthesis of nanoscale ZnO materials has greatly improved the specific surface area of ZnO and increased the adsorption active sites of the gas to be measured, which provides an important idea for room temperature sensing. Au, Pd, Pt and other precious metals have strong catalytic activity, and high conductivity. Doping precious metals into ZnO semiconductors can effectively improve the sensitivity at room temperature. ZnO is a typical n-type semiconductor. Doping with SnO_2 and other p-type semiconductor materials can form a thicker electron depletion layer to improve its response value [46]. Graphene has high specific surface area and good conductivity. The composite of ZnO and graphene is also an important strategy to improve the room temperature sensing performance. Optical excitation can effectively improve the carrier concentration of ZnO at low temperature. More and more attention has been paid to the sensing of

ZnO Gas sensors at room temperature by introducing different wavelengths of light such as ultraviolet and visible light.

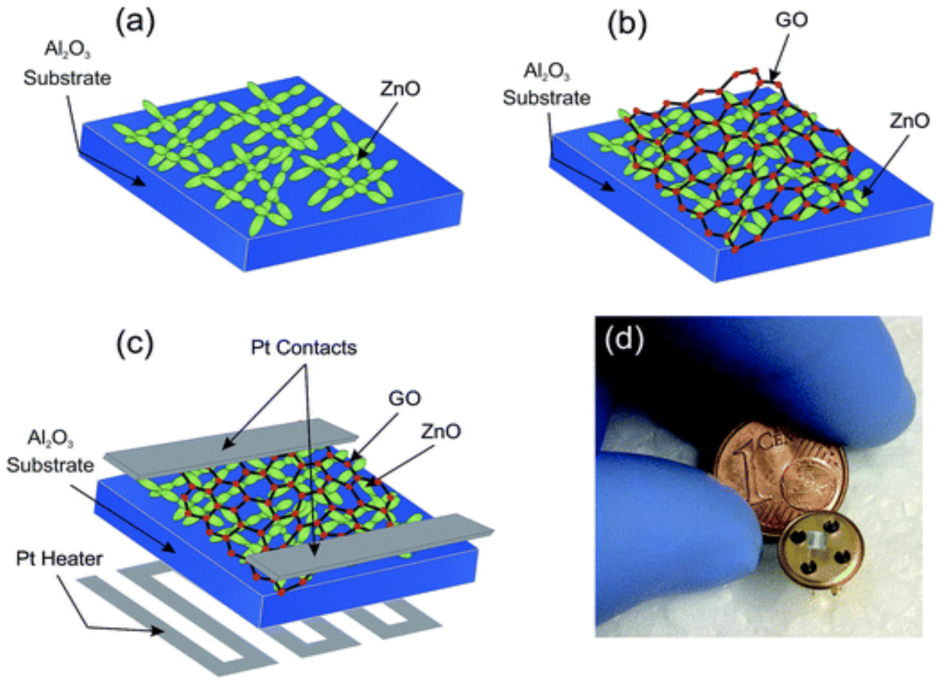

Figure 1.9 ZnO nanoparticle used in Gas sensor application [47]

Catalysts and photocatalysts

Due to the small size, large specific surface area, different bond states between the particle surface and the interior, barrier free surface atomic coordination and other reasons, the active sites on the surface of ZnO nanomaterials increase, resulting in uneven atomic steps and increased reaction contact surface. It is expected that ultrafine particle catalysts will play an important role in catalytic reactions in the next century. ZnO nanomaterial is also a good photocatalyst. Under ultraviolet irradiation, it can decompose organic matter and has antibacterial and deodorizing effects. This photocatalytic performance has been widely used in fiber, cosmetics, ceramics,

environmental engineering, glass and building materials industries. Asma Tabib et al. [48] studied the photocatalytic degradation activity of undoped and sodium doped ZnO nanocrystals (NCs) on rhodamine B (RhB) aqueous solution under solar light to prove its environmental application potential in removing pollutants from wastewater. Figure 1.10a shows the change of absorption spectrum of an RhB aqueous solution (5×10^{-6} M) as a function of irradiation time in the absence and presence of ZnO NCS. The photodegradation of RhB aqueous solution was evaluated by UV-vis absorption spectroscopy by controlling the attenuation of the absorption peak at 554 nm as a function of irradiation time. After 120 minutes of irradiation under sunlight, the direct irradiation of RhB without photocatalyst resulted in about 15% degradation (Figure 1.10a). Adding ZnO photocatalyst to RhB aqueous solution can improve the photodegradation efficiency, and the degradation rate after 120 minutes is 84.4% (Figure 1.10b). Interestingly, the 0.5% Na doped ZnO NCS shown in Figure 1.10c almost completely degraded RhB after 90 minutes of sunlight.

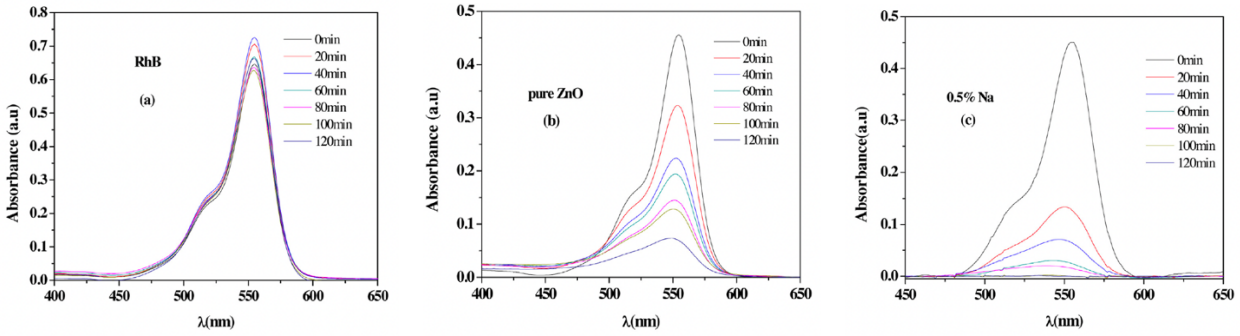

Figure 1.10 UV–vis absorbance of RhB during photocatalytic degradation under solar irradiation in the absence of photocatalyst (a) and presence of undoped ZnO (b) and 0.5% Na-doped ZnO NCs (c) [48]

Stealth technology - radar wave absorbing material

Radar wave absorbing materials (radar absorbing materials for short) is a kind of functional material that can effectively absorb human radar waves and make them scatter and attenuate. It has great significance in national defense. The development and application of this "stealth material" is an effective means to improve the survival and penetration ability of weapon systems. Nano powder is a new type of military radar wave absorber with great development prospects. Due to their light weight, thin thickness, light color, and strong absorbing ability ZnO nanomaterial and other metal oxides have become one of the research hotspots of microwave absorbing materials.

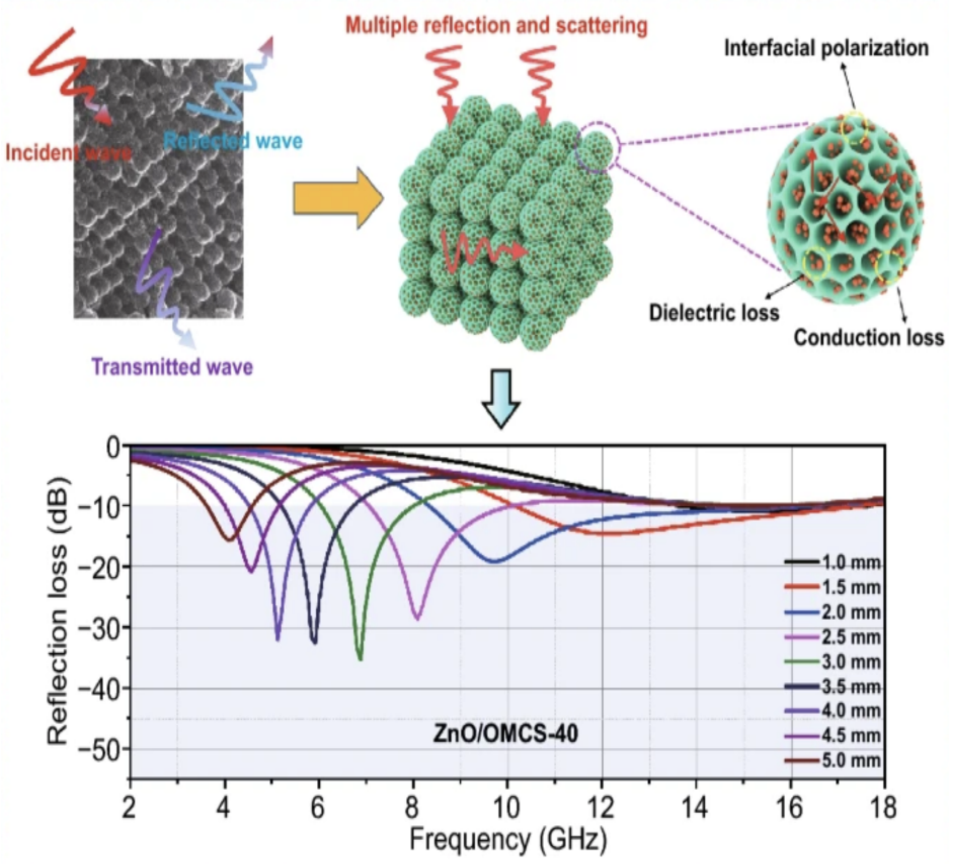

Figure 1.11 ZnO nanoparticle used in radar wave absorbing material [49]

Application in cosmetics -- new sunscreen and antibacterial agents

ZnO nanoparticles also exhibit great UV barrier properties. Generally, sunlight consists of three types of ultraviolet radiation, namely UV-A (320-400 nm), UV-B (290-320 nm) and UV-C (250-290 nm). UV-A radiation is the main problem because it contributes to 95% of the total solar radiation. UV-B radiation contributes ~ 5%, while UV-C radiation has no significant effect because it is absorbed by ozone on the earth's surface [50]. In recent years, the United States, Japan, Germany, Britain, Australia, and other countries are actively developing sunscreen. In the United States, more than 50% of cosmetics are added with sunscreen. In the past, most sunscreens were organic compounds, but in recent years, some inorganic sunscreens such as zinc oxide nanomaterials, titanium and iron oxide red have been favored. It is widely used because it is non-toxic, tasteless, non-irritating to the skin, does not decompose, does not deteriorate, and has good thermal stability. ZnO nanomaterials are white, simple color, cheap price, strong ultraviolet absorption capacity and can shield UV-A and UV-B. Siddiquey et al. [51] reported the synthesis of silica coated ZnO nanoparticles by microwave-assisted route and proved its photocatalytic activity. The figure 1.12 shows the UV–visible absorption spectra of different nanoparticles.

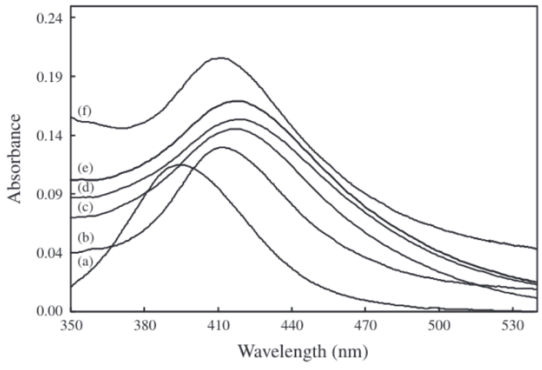

Figure 1.12 UV–visible absorption spectra of: (a) 17 nm uncoated Ag nanoparticles and Ag@SiO_2 nanoparticles prepared by MW technique at TEOS concentration of (b)0.5 mM, (c) 1 mM, (d) 2 mM, (e) 3 mM, and (f) 4 mM [51]

ZnO nanomaterials can decompose free moving negative electrons (E-1) and leave positive holes (H) in water and air (oxygen) under sunlight, especially under ultraviolet radiation. This kind of hole can activate the oxygen in the air to become active oxygen. It has strong chemical activity and can react with a variety of organic substances (including organic substances in bacteria) to kill most bacteria and viruses. Therefore, adding ZnO nanoparticles in cosmetics not only can shield ultraviolet rays and sunscreen, but also can resist bacteria and deodorize.

1.3 Main Factors Affecting Gas Sensor Sensitivities

As one of the important parameters of gas sensors, sensitivity has been paid increasingly attention. A lot of work has been done to improve the sensitivity of gas sensors. At present, the definition of gas sensor sensitivity is not unified. Generally, the sensitivity can be defined as $S=R_a/R_g$ or $S = \Delta R/R_g$ for reducing gas and $S = R_g/R_a$ or $S = \Delta R/R_a$ for oxidizing gases, where R_a is the resistance of the gas sensor in the reference gas (usually air) and R_g is the resistance in the reference gas containing the target gas [52]. In addition to sensitivity, response time and recovery time are also the main performance parameters of the gas sensor. Response time is defined as the time required for the sensor to reach 90% of the total signal response (such as resistance) when exposed to the target gas. Recovery time refers to the time required for the sensor to recover to 90% of the original baseline signal after removing the target gas [53]. The sensitivity of the gas sensor

is affected by many factors, such as materials, nanostructure, surface areas, surface additives, temperature, humidity, light sources, etc.

1.3.1 Film Morphology and Surface Characteristics

The morphology of sensing film is an important feature of gas detection. It is recommended to use a porous surface with smaller particle size and higher surface roughness to obtain better gas sensitivity. For most articles, the film morphology is usually studied through different sections, such as surface roughness, particle size, porosity, photoluminescence spectra, Raman spectra, EDX spectrum etc.

Particle size

Many studies have found that the particle size of nanostructured ZnO has a significant impact on its sensor response. The response greatly depends on the particle size when it is close to or less than twice the debye length (space charge layer depth) and can increase exponentially with the decrease of grain size [54]. When the particle size is much larger than twice the debye length, the gas sensitivity is controlled by the contact barrier rather than the particle size. There are many studies that have focused on reducing the particle size of nanostructured ZnO to improve the gas sensing performance, and the particle size usually analysis or study through AFM (Atomic Force Microscopy), SEM (Scanning Electron Microscope) or FESEM (Field Emission Scanning Electron Microscopy) micrographs (Figure 1.13). However, the particle size cannot be reduced blindly because the particle size is inversely proportional to the van der waals force promoting particle agglomeration, it not only reduces the specific surface area, but also limits the gas diffusion

between particles. In addition, the much smaller particle size ZnO is usually accompanied by a decrease in thermal stability.

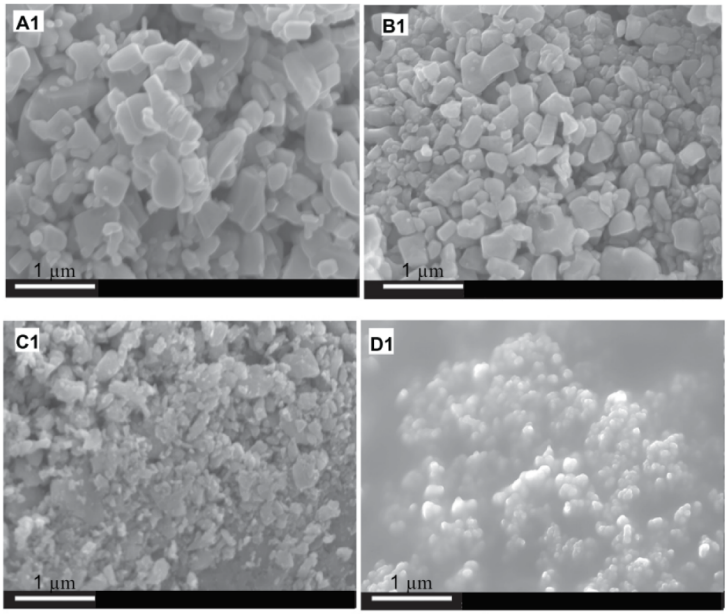

Figure 1.13 Typical FESEM micrographs of ZnO powders in two magnifications; (a and b) as received and (c and d) after mechanical milling for 8 h. [20]

Surface Roughness

The surface roughness is determined by the distance between peaks and valleys. The farther the distance, the rougher the surface. AFM measurements (Figure 1.14) can provide valuable information about the properties of deposited films, such as roughness and particle size. When the film is formed, detailed analysis of roughness can obtain information about growth and nucleation. In most articles, the root-mean-square roughness (RMS) is defined as $RMS(nm)=[\sum(z_i-z_{ave})2/N]^{½}$ where z_i is the current value of z, z_{ave} is the mean value of z in the scan area, N is the number of points [55].

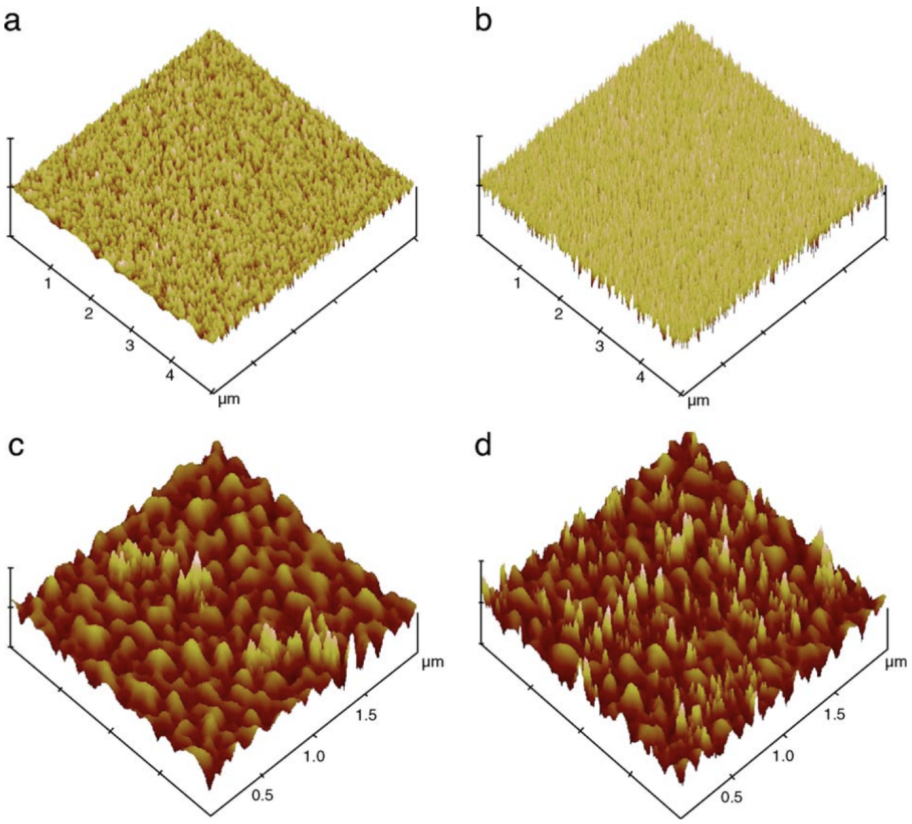

Figure 1.14 AFM 3D images of as-deposited ZnO thin films at room temperature with Ar ratios of respectively (a) 0%, z-range 50 nm/div (b) 27% from Zn metallic target-range 50 nm/div (c) 100%, z-range 30 nm/div (d) 90% from ZnO ceramic target, z-range 30 nm/div. [55]

Photoluminescence spectra (photoluminescence spectroscopy)

Photoluminescence spectrum, commonly known as PL, refers to the photon emission of any substance stimulated by light energy or photons. This is a non-contact and non-destructive material detection method. In essence, light is directed to the sample, where it is absorbed, where a process called light excitation can occur. Photoexcitation causes the material to transition to a higher electronic state and then release energy (photons) because it relaxes and returns to a lower energy level. The light or luminescence emitted through this process is called photoluminescence.

Therefore, photoluminescence spectra are always used to study the morphology and surface characteristics in most of the articles. When the size of semiconductor materials is reduced to nanoscale, their physical properties will change, which is called "quantum size effect". Photoluminescence originates from the recombination of surface states. Strong PL means that the surface state is still very shallow, because it is reported that the quantum yield of the band edge will decrease exponentially with the increase of the energy level depth of the surface state [56]. Figure 1.15 shows an example of the photoluminescence spectrum of ZnO nano powder with an excitation wavelength of 320 nm at room temperature [57]. The spectrum shows two emission peaks, one at about 392 nm (UV region) corresponding to near bandgap exciton emission [58], and the other at about 520 nm due to the existence of a single ionized oxygen vacancy

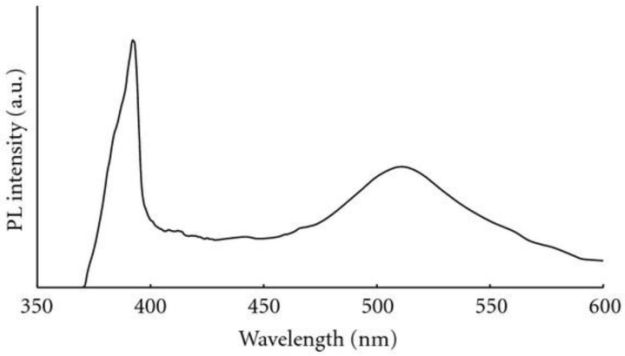

Figure 1.15 Photoluminescence spectrum of prepared ZnO nanoparticles (λ = 320nm) which shows two emission peaks, one at about 392 nm corresponding to near bandgap exciton emission, and the other at about 520 nm, due to the existence of single ionized oxygen vacancy. [57]

Raman spectra

Raman spectra is another important way to study the film morphology and surface characteristics. Raman spectroscopy is a light scattering techniques, which is usually used to

determine the vibrational modes of molecules and solids, including rotational modes and other low-frequency modes of the system being studied. Raman spectroscopy is often used in chemistry to provide structural fingerprints through which molecules can be identified. Raman spectra of ground and mechanically activated zinc oxide powders are shown in Figures 1.16. The Raman characteristics of inactivated ZnO powder (block) are attributed to the Raman active mode of ZnO wurtzite crystal [59]. Wurtzite ZnO belongs to the space group p63mc, and each original cell has two formula units. The region center optical phonons can be classified according to the following irreducible representations: $\Gamma_{opt} = A_1 + E_1 + 2E_2 + 2B_1$, where B_1 mode is silent mode, A_1 and E_1 are polar modes, Raman and infrared are active modes, while E_2 mode (E_2 low and E_2 high) is only non-polar and Raman active modes [59].

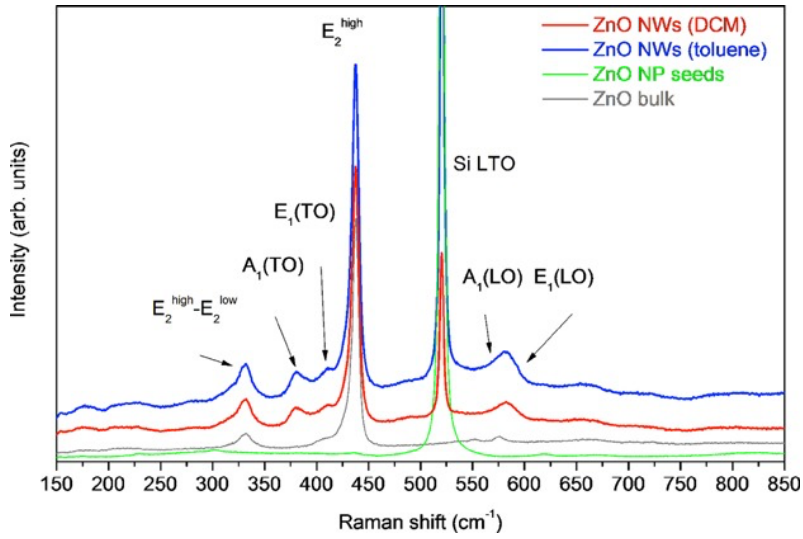

Figure 1.16 Raman spectra of the ZnO NWs (DCM in red or toluene in blue) on a SiO2/Si substrate. ZnO NP seeds (green) and ZnO bulk c-plane (gray) as comparison. [60]

1.3.2 Operating temperature

Operating temperature will control reaction kinetics, conductivity and electron mobility which will affect the gas sensing performance of ZnO based gas sensors. Normally, traditional ZnO gas sensors work at high temperatures of 300-500 ℃, because sufficient surface redox reaction heat energy is needed to overcome the activation energy barrier and increase the reaction kinetics to realize sensing measurement. However, high temperatures will cause energy waste, and gas explosions when measured gases which have the low ignition point of flammable and explosive under the normal atmosphere. In addition, due to the high working temperature, it is easy to produce heat induced ZnO grain growth, which affects the gas diffusion at the grain boundary, is the reason for the bad long-term drift problem caused by sintering effect, and sensor instability that shortened the service life, which may lead to inaccurate or incorrect test results. Therefore, it is an urgent need to reduce the working temperature of the ZnO based gas sensor. Room temperature operation can reduce energy consumption, the risk of gas explosion, and improve long-term stability, which has become a continuous development topic. Zinc oxide-based gas sensors work at room temperature without a heating device which makes the gas sensor more portable and cost-effective.

1.4 Project Outline

In this report, we have studied the electronic properties of zinc oxide, and produced gas sensor samples using thin films of zinc oxide prepared via planetary ball milling (PBM) and doctor blading of the resultant slurry (or nanoink). We have measured their gas response under varying grinding parameters (speed, time, and solvent), different thin film samples with different particle

size and porosity and tested with dry air against argon, nitrogen and hydrogen as testing gas. In addition, we tested our sensor under different relative humidity and different ambient light conditions. Chapter 1 clarifies the motivation and background for the rest of this report by introducing some of the challenges in the semiconductor industry, the need for new material applications, and the characteristics and potential applications that make ZnO an interesting research material. Chapter 2 mainly introduces the experimental methods used in this study. We start with the manufacturing method of planetary ball mill, after describing the process and its parameters. Then we have introduced a thin film sensor produced by the doctor blading method, introduced the system we are using to do the experiment and used to collect data about the gas sensor under different testing gases, operating temperature, humidity and light condition. These data will be analyzed in the next chapter (chapter 3), which will provide the main results of the study (the result of this report has published in the article "Thin film gas sensors based on planetary ball-milled zinc oxide nanoinks: Effect of milling parameters on sensing performance" [61]). Here, we discuss the observable behavior we obtain by controlling various parameters. The effect of oxygen, light, humidity, grinding speed and grinding time on the conductivity of the ZnO thin film was studied. Finally, in Chapter 4 we put forward some suggestions for the future work to continue the research direction of this report. Some of the results of this work are published in an article on thin film gas sensors.

Chapter 2

Experimental Setup and Procedure

2.1 Materials of Gas sensor

2.1.1 Method of Fabrication: Planetary Ball Milling

Nano grinding is an efficient top-down mechanochemical method to prepare nanomaterials. In a range of industries, obtaining smaller particle sizes is one of the most important unit operations because of the advantages gained through this material change. For any given mass of material, a smaller particle size results in a larger net surface area. This gain is ideal when the surface area is important due to its chemical properties. Usually starting from the powder form, a material is subjected to multiple high-energy shocks, which decompose particles into smaller and smaller sizes. Due to the high energy at the point of impact, chemical changes may also occur in the material because the bonds are broken and reformed. Therefore, high-energy ball milling is called mechanochemical synthesis technology [24]. High energy ball milling has become an important way to prepare nanomaterials. With the deepening of research, it is not only widely used to prepare new metal materials, but also used to prepare amorphous materials, nanomaterials, and ceramic materials, which has become a very important method in the field of material research.

The grinding methods of laboratory ball mills include planetary type, roller type, stirring type, and etc. The grinding methods include dry grinding and wet grinding, while the ordinary ball mill and high-energy ball mill are distinguished by the energy contained in the ball grinding. At present, there is no relevant standard for ordinary ball milling and high-energy ball milling, but some people classify planetary ball milling as high-energy ball milling. Planetary ball mill is

widely used in high-energy ball milling such as mechanical alloying. The higher speed of the planetary ball mill is more than 1000r / min for the same size ball mill machine. Planetary ball mill is the interaction of various centrifugal forces, the planetary structure makes a variety of forces balanced, always able to effectively grind, most of the energy used in ball milling.

Planetary ball mill is widely used in sample processing, colloid grinding and material development due to its good reproducibility, safe operation, and short processing time. Planetary ball mills have a history of more than 100 years. Normally, there are 2 to 4 pots placed on a planetary disk for grinding materials. The jar is connected to a disk that rotates around a common central axis, while the jar rotates around its axis. The high rotation speed of the bowl and disc results in the high impact energy of the ball in the bowl, which can achieve effective grinding performance. In the MA process, the crushed materials are mainly powder particles, which are located between the surface and the surface that are crushed due to the impact force or friction caused by a collision [21]. The powder particles are trapped between the collision balls, which makes the collision inelastic, thus slowing down the movement of the ball and reducing the energy dissipation [62]. The movement of the ball will affect the number of collisions and the speed of the ball, which will affect the impact strength of the ball, and the impact strength of the ball is helpful to input energy into the powder charge. In the process of machining, the grinding ball shows complex motion behavior in the grinding chamber, and its motion law changes with the change of operating parameters. With the increase of filling ratio and rotating speed, it changes from cascade to cracking, then to centrifugation or rolling [23].

The scheme of a ball motion pattern in a single pot of a planetary ball mill is shown in Figure 2.1 below. In the cascade state (Fig. 2.1a), the grinding balls are carried away by the tank wall and spread out from the top to the bottom of the main body, while in the cataracting state, the

grinding balls separate from the tank wall and impact the main body or the opposite side wall with high strength. The rolling or centrifugal ball rotates towards the wall with little relative velocity [21].

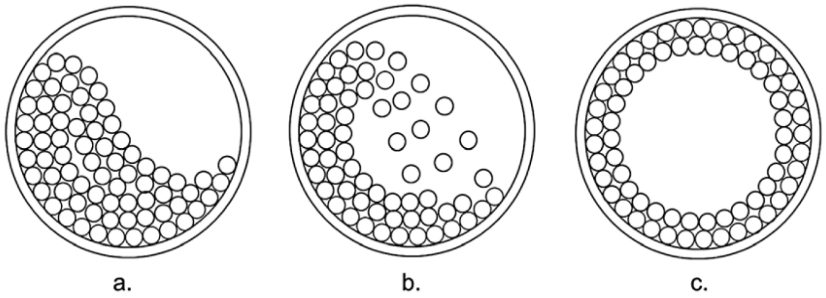

Figure 2.1 Scheme of a ball motion pattern in a single pot of a planetary ball mill –

(a) cascading, (b) cataracting, (c) rolling. [21]

Although high energy ball milling requires less equipment and a simple process, but there are many factors affecting the final product composition and performance.

The Ratio of Ball to Powder

The ratio of ball to powder refers to the mass ratio of material and grinding body in the ball mill, which is an important parameter affecting the ball milling process. If there are few numbers of balls, the times of impact and grinding will not be enough, that let to low efficiency. If it is too much, the impact between balls will be affected, and the crushing effect will not be brought into full play.

Amount of Dispersant

In the process of rapid ball milling, the electrostatic friction caused by the high-speed collision among powder, small ball and tank wall makes some powders stick to the pipe wall and small ball, and then form large particles; the added dispersant can be adsorbed on the surface of the powder, which can reduce the surface activity and weaken the ability of powder aggregation.

Grinding Speed

The higher rotational speed of the ball mill, the more energy will be transferred to the grinding material, but a higher speed does not necessarily mean a better way. This is because, on the one hand, when the rotation speed of the ball mill increases, the rotation speed of the ball milling medium will certainly increase. When it reaches a certain critical value or above, the centrifugal force of the ball is greater than gravity, and the ball milling medium is close to the inner wall of the ball milling container, and the ball, powder and grinding cylinder are in a relatively static state. At this time, the ball milling stops, and the ball milling material does not produce any impact, on the other hand, too high rotational speed will make the temperature of the ball milling system rise too fast, which is sometimes disadvantageous, for example, a higher temperature may lead to the decomposition of supersaturated solid solution, amorphous phase or another metastable state.

Grinding Time

The length of ball milling time directly affects the composition and purity of products, on particle size, the effect of ball milling time is also obvious. In the initial stage, with the extension of time, the particle size decreases rapidly, but after a certain time, even if the ball milling time

continues to extend, the particle size value of the product decreases very little. Therefore, under certain conditions, with the process of ball milling, the alloying degree will be higher and higher, the particle size will gradually reduce, and finally to a stable equilibrium state, at this time the particle size will not change. On the other hand, the longer the milling time is, the pollution will be more serious, which will affect the purity of the product.

Grinding Medium

In ball milling, stainless steel is generally used as the milling medium. To avoid the pollution of the milling medium to the samples, ceramic balls are also used in milling some materials with good grindability. Ball milling media should have appropriate density and size, to produce enough impact on the material, which has a direct impact on the final product after ball milling.

Other Factors

The influence factors of high energy ball milling methods are ball milling temperature, ball milling atmosphere, process control agent and so on. It is generally believed that temperature affects the diffusion rate of crystal, and ultimately affects the performance of nanomaterials; the ball milling process is generally carried out under the protection of vacuum or inert gas, to prevent the pollution of the gas environment; the role of the process control agent is to prevent powder agglomeration, speed up the ball milling process, and improve the powder yield. Common process additives include stearic acid, solid paraffin, liquid alcohol, and carbon tetrachloride.

In this project, we control the speed of the milling process while trying to keep other parameters of a given material/batch unchanged. The grinding procedure is carried out in a Fritch Pulverisette 7 planetary ball mills (premium line) as shown in Figure 2.2. This machine is equipped with 2 grinding stations, which is suitable for a wide range of applications and wear-free grinding of hard, medium, and brittle materials to a final fineness of 100 nm. The jar is made of silicon nitride with a capacity of 80mL. The ball used for grinding is a 2mm diameter bead of zirconia. Generally, the ratio of ball to powder is 20:1. The weight of all grinding balls is 100g, zinc oxide powder (~7g) is ground in approximately 10ml of glycol or deionized water (DI water) solution (also known as gel grinding).

Figure 2.2 Fritch Pulverisette 7 planetary ball mills

Grinding speed and time varies between 200 and 1,000 rpm, between 10 and 60 minutes (grinding cycle 5 minutes; rest cycle 5 minutes). Rest time is necessary as heat quickly accumulates from the friction in the can. It is also useful to perform routine checks on the jar. Based on experience with pressure build-up in the tank, the following practices were carried out when

performing the grinding procedure - checking the seal of the tank during break time and after trials to detect any leakage that may occur. The rest time increased in the case of trials with higher speed. The details of each trial are shown in table 2.1 below.

Trial	Speed (rpm)	Duration (mins)	Rest-time (mins)	Dispersant
EG-200a	200	10	5	EG
EG-400a	400	10	5	EG
EG-600a	600	10	10	EG
EG-800a	800	10	10	EG
EG-1000a	1000	10	15	EG
DI-200-10	200	10	5	DI water
DI-200-30	200	30	5	DI water
DI-200-60	200	60	5	DI water

Table 2.1: Parameters of the grinding trials

2.1.2 Materials

In this project, the main material is zinc oxide (ZnO), which is ground under various parameters discussed later. The ZnO powder used is 99% pure and produced by Anachemia Canada Inc. ZnO nanoparticles with controllable size and structure are necessary to study their size dependent properties and explore their applications in various fields of nanotechnology [63].

In various studies, zinc oxide powder was reduced to nanoscale by ball milling under different grinding times and grinding speed.

Zinc oxide is a widely used and multifunctional wide bandgap semiconductor material and one of the most promising materials. ZnO thin film has many properties, such as photoelectricity, piezoelectricity, pressure sensitive and gas sensitive, which makes it widely used in transparent conductors, light-emitting devices, solar cells, optical waveguide, single color field emission display, high-frequency piezoelectric converter, micro sensors, and other aspects [64-66]. ZnO is one of the earliest and most widely used semiconductor gas sensitive materials, which has good sensitivity to a variety of gases at a suitable temperature. Compared with the other two metal oxide gas sensitive materials SnO_2 and Fe_2O_3, ZnO has better stability, but lower sensitivity and higher working temperature, generally 400~500 °C [67]. With the development of automatic control, automatic detection and other technologies, the demand for gas sensors with excellent performance is increasing.

In this project, we use a ZnO thin film gas sensor, which is exposed to different gas species when operated under room temperature through the change of resistance, testing the effects on the structure and electrical properties of the nanoparticles of the synthetic film by changing the grinding parameters (grinding speed, grinding time and solvent).

2.2 Preparation of Zinc oxide thin film

2.2.1 Doctor Blade method

The doctor blade method is a widely used technology for the preparation of thin films on a large area of surface. In general, during the process, a slurry consisting of a ceramic particle suspension and other additives such as adhesives, dispersions or plasticizers is placed on a base other than the doctor blade. When a constant relative movement is formed between the blade and the substrate, the slurry spreads on the substrate to form a sheet, and a gel layer is formed after drying. The layer is formed by a doctor blade that is either stationary when used with a moving casting surface, or by a frame that moves along a stationary casting surface. The principle is shown in figure 2.3 [68]

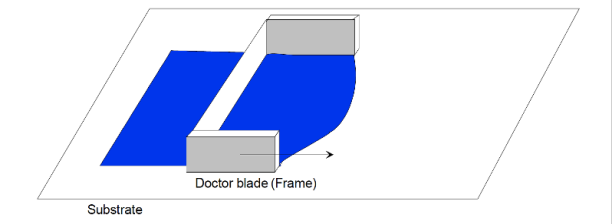

Figure 2.3 Principle of doctor blading using a frame with a reservoir of coating liquid which is moving relatively to the substrate. [68]

The thickness of the layer is determined by adjusting the gap between the doctor blade and the substrate, as it is shown in figure 2.4. The thickness of the thin film can also be controlled by using tape upon the edges for different numbers of tapes, such as 1 tape for 5 μm, 2 tapes for 10 μm, 3 tapes for 15 μm, etc. [69]

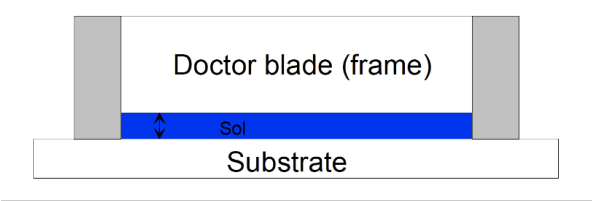

Figure 2.4 The thickness of the thin film layer (blue part) control by the gap between the frame and the blade. [68]

In our experiment, we have prepared the thin film using doctor blading method with a razor blade (the blade used to create thin film) and use scotch tape to make casting surface on the thick glass substrate as required, ensure tape adheres well to the surface and there are no bubbles. The thickness of the film is also controlled by the thickness of the scotch tape was approximately 60 µm. Drop around 5-10 µL of the suspensions using a micropipette and apply it on one side of the substrate (just outside of area to be coated). Then dry the film on a hot plate for 5-10 min at 130˚C for quick drying. Finally, remove the scotch tape carefully after film is dried and the thin film sample is shown in Figure 2.5.

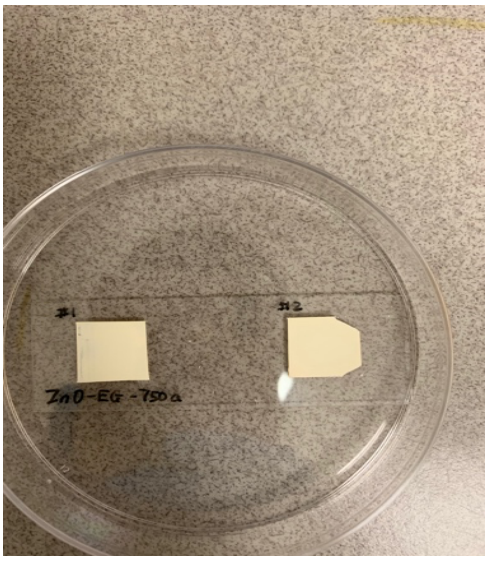

Figure 2.5 ZnO thin film sample prepared using doctor blade method.

2.2.2 Thin film gas sensor samples

A plurality of thin film samples for each ground ZnO test were prepared on the substrate using a blade for characterization as follows: several samples were used μL ZnO nanoink, the surface is coated by sweeping a scraper across the substrate (covered with a single layer of transparent tape) and the suspension (scraper angle 20-30°). The coating is dried on a heating plate at a temperature of about 100 °C for about 5 minutes. To make the gas sensor device, two electrical contacts were connected to the final film using silver paint and copper tape (see Fig. 2.6) and then dried in a mechanical oven at 75 ℃ for 10-15 minutes.

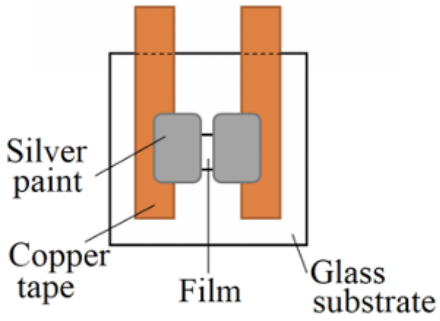

Figure 2.6 Schematic diagram of thin film gas sensor device: copper strip (including doctor blade ZnO film) on glass substrate is used as electrode contact, and silver paint is used to connect the sensor film to the electrode

2.3 Experiment system set up

Gas sensitivity studies were carried out at ambient pressure and temperature (approximately 22 °C) using the set up shown in Figure 2.7, which consists of a quartz tube

chamber connected to a precision power measurement system (Keithley 4200-SCS) and a compressed gas source (target / carrier species) through a mass flow controller. The double ended resistance, current voltage (I-V) characteristics and the relationship between the response and applied bias/time of the ZnO thin film sensor in different gas environments were measured. Before injecting the target gas into the room, the baseline behavior of the sensor in the dry air carrier gas was found. Measure the relative humidity (RH) in the test room using a pre-calibrated temperature and humidity meter Digi Sense 20, 250-11.

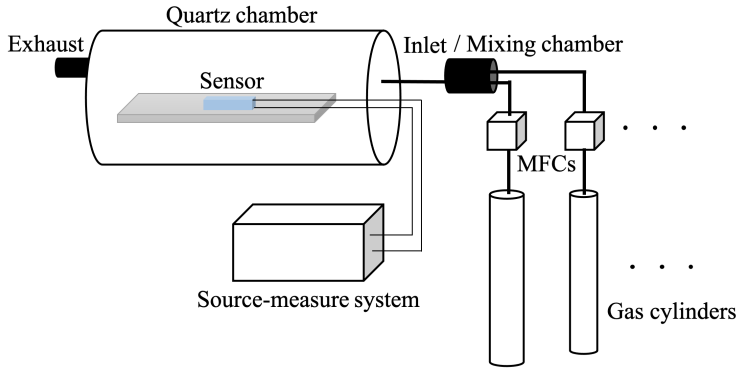

Figure 2.7 Illustration of the gas sensing device used. The sensor is placed in a quartz chamber and connected to the gas cylinder (carrier or target gas) through the mass flow controller. The copper wire is connected to the sample through sealed leads for electrical measurement. The electrical response of the sensor is monitored using a precision source measurement system.

SCCM and PPM conversion

In addition, the unit of mass flow controller is standard cubic centimeters per minute (SCCM), we need to convert it to parts per million (ppm) to calculate the concentration of target gases. First, we convert the SCCM to atom/s for an ideal gas with following equation:

$$1\ \text{sccm} = \frac{6.02214179 \times 10^{23}\ [\frac{\text{atoms}}{\text{mole}}]}{22.413996[\frac{\text{liters}}{\text{mole}}] \times 10^{3}[\frac{\text{cc}}{\text{liter}}] \times 60[\frac{\text{s}}{\text{min}}]} = 4.477962 \times 10^{17}[\frac{\text{atoms}}{\text{s}}]$$

Given 6.02214179 x 10^{23} atoms/mole is the Avogadro's number, and 22.413996 is the molar volume of ideal gas at standard press and temperature.

Then, we could convert 100 SCCM testing gas by using the equation below, since our testing chamber has the volume of 1 mole, the result $4.477962 \times 10^{17}\left[\frac{\text{atoms}}{\text{s}}\right]$ can be used to our conversion calculation.

$$\frac{4.477962 \times 10^{17}[\frac{atoms}{s}] \times 100\ sccm\ \times 60s}{6.02214179 \times 10^{23}\ [\frac{atoms}{mole}]} \times 10^{6} \approx 5000\ ppm$$

Given 6.02214179 x 10^{23} atoms/mole is the Avogadro's number, and the transit time inside the chamber is approximately 60s.

2.4 Summary

In this report, we have been grinding the ZnO powder into nanoparticles using planetary ball milling as the nanofabrication technique. In order to test the properties and effects with different grinding parameters, we have prepared them with different grinding speeds (200 - 1000

rpm), grinding times (10 - 60 min) and solvents (DI water and ethylene glycol) and extracted them into different vials, shake and sonicate vials before fabricating the thin film. To prepare the gas sensor samples, we fabricated thin film using a doctor blade method (the details are shown in sections 2.2.1 and 2.2.2) and using silver paint and copper tape as the connection to the two electrical contacts. To test the gas sensing properties, we have set up an experimental system using a quartz tube chamber connected to a compressed gas source (target/carrier species) through a mass flow controller. Two-terminal resistance, current-voltage (I-V) characteristics, and response versus applied bias/time of the thin film were measured in different gas environments in a Keithley 4200 SCS.

Chapter 3

Result and Discussion

In this project, we are mainly focused on testing the effects on the nanoparticle structure and electrical properties of the ZnO thin film gas sensors by changing the grinding parameters (grinding time and grinding speed) and operating at room temperature, which through resistance changes when exposed to different gas species. Next, we will show the result of two-terminal resistance, current-voltage (I-V) characteristics, and response versus applied bias/time of the ZnO film sensors were measured in different gas environments.

3.1 Film morphology and material characterization

To verify our film morphology and surface characterization, a Nanonics MultiView 1000 atomic force microscope (AFM) with Olympus BXFM optical microscope was used. In addition, the thin film samples were measured by Raman scattering using Renishaw inVia Raman microscope. Raman spectra were collected by the 632.8 nm HeNe laser line under ambient conditions. Photoluminescence (PL) spectra were obtained by Olympus FV1000 confocal laser scanning microscope using a solid-state laser line with a wavelength of 405nm. Scanning electron microscopy (SEM) and energy dispersive X-ray analysis (EDX) were performed using HITACHI S-2600.

In Figure 3.1, it shows an optical microscope image of a typical ZnO thin film coating formed, which using PBM nanoink and doctor blade method. The coating exhibits good uniformity, stability and adhesion under ambient conditions and temperatures up to 200 °C. The SEM image in Figure 3.2 shows that the ground ZnO film is composed of fine nanostructured particles with distributed pores. The surface morphology of ZnO film was further characterized by AFM (Figure

3.3) as expected. With the increasing of grinding speed, the particles were ground to finer size. We observed that the root mean square (RMS) film roughness decreased. As measured by AFM (Figure 3.4) after grinding for 10 minutes at 1000 rpm, the root mean square (RMS) film roughness decreased below 80 nm. The higher grinding speed also reduces the particle size below 100 nm (Figure 3.5) With the increase of grinding time (at constant speed), a similar downward trend of particle size/film roughness was observed (see Figure 3.6) [70]

Figure 3.1 An optical microscope image of doctor bladed ZnO thin film on glass substrate.

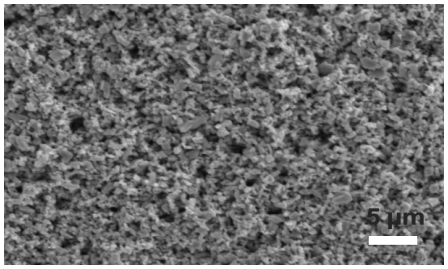

Figure 3.2 SEM image of milled ZnO nanoparticles ground with DI water at 200 rpm for 30 min.

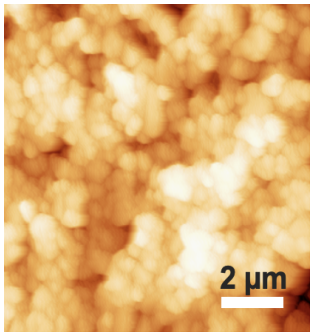

Figure 3.3 AFM images of ZnO film prepared using PBM nanoinks with DI water ground at 200 rpm for 10 min.

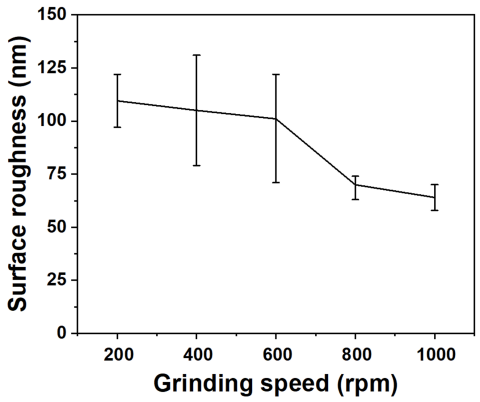

Figure 3.4 Plot of RMS roughness from AFM of ZnO thin films using PBM nanoinks ground in EG for 10 min. at different speeds.

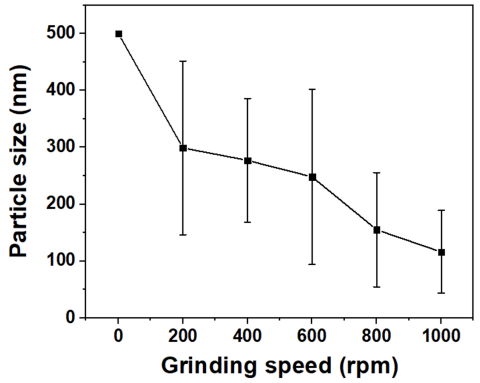

Figure 3.5 Average particle size of ZnO PBM nanoinks ground using EG for 10 min. at different speeds

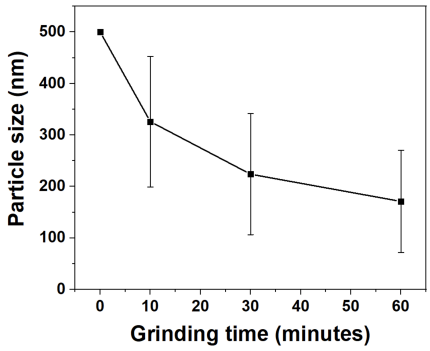

Figure 3.6 Average particle size of ZnO PBM nanoinks ground using DI water at 200 rpm for different grinding time

The photoluminescence spectra of typical films are shown in Fig. 3.7. The ground ZnO film shows five different peaks with different intensity levels in different wavelength ranges, which is related to the electronic and structural properties of the ground particles: consistent with previous studies, the 465 nm peak (blue emission band) is attributed to the deep-level emission of oxygen vacancies or interstitial zinc ions from ZnO [71]. Green emission (525 nm) is due to single ionized oxygen atoms or oxygen anti site defect O_{Zn} [63]. Similarly, the peak at 577 nm is probably due to the disorder of the surface of nanoparticles after grinding [63]. Finally, the other 590 nm and 650 nm emission peaks are usually attributed to oxygen vacancies [72].

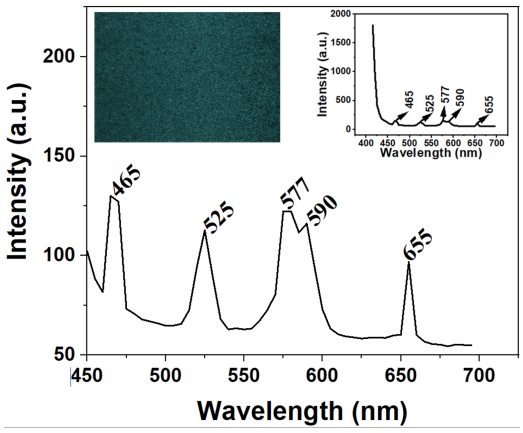

Figure 3.7 Photoluminescence spectra between approximately 450-700 nm of ZnO thin film ground at 200 rpm for 60 minutes using DI water solvent; (inset (left) optical map image of total PL intensity obtained between 415-715 nm and (right) overall range averaged full spectrum).

The Raman spectra of PBM nanoink film and bulk starting powder are shown in Figure 3.8 and Figure 3.9. ZnO usually has wurtzite structure. In the Raman spectrum of its crystal structure, there are two A1, two E1, two E2 and two B1 modes [60]

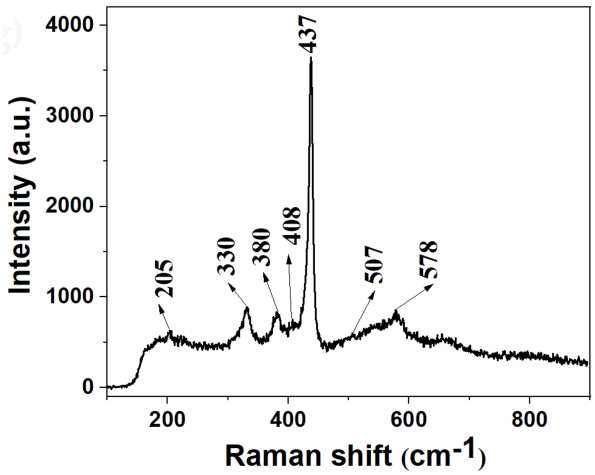

Figure 3.8 Raman spectra of ZnO ground film prepared using DI water ground at 200 rpm for 60 minutes.

The most common Raman intensive E2 (low) mode at about 99 cm^{-1}, that is just beyond our detection range. However, another Raman mode E2 (high) at about 437 cm^{-1} is visible, which is designated as oxygen vibration mode [56]. E2 (high) mode is the most prominent in the starting material, and the peak strength decreases and widens after ball milling. The decrease of intensity and broadening of 437 cm^{-1} peak indicate that the energy band structure and crystallinity of nanostructures change after grinding. The Raman spectra of ground and bulk powders show three different peaks at about 206, 329, 379 and 412 cm^{-1}, which are attributed to 2TA:2E2, E2(high)-E2(low), A1(TO) and E1 (TO) symmetry, respectively [56]. However, the wider Raman peak and lower intensity are attributed to size effect, lattice strain and lower crystallinity [63]. During ball milling, the decrease in crystallinity is attributed to defects produced. For the milled nanoparticles, there was a more and more obvious wide peak at about 580 cm^{-1}. With the extension of grinding time or the increase of grinding speed, the peak became wider and more obvious. It is predicted that high intensity peaks of 560 to 580 cm^{-1} indicate the presence of defects related to oxygen vacancy (V_o) and / or zinc gap (Zn_i) [56, 73]. Grinding

media (grinding beads, solvents) can also affect particles, but the significant may only for longer grinding times and/or higher speeds (see red curve Figure 3.9 – the peak at 189 cm^{-1} is related to zirconia grinding beads [32])

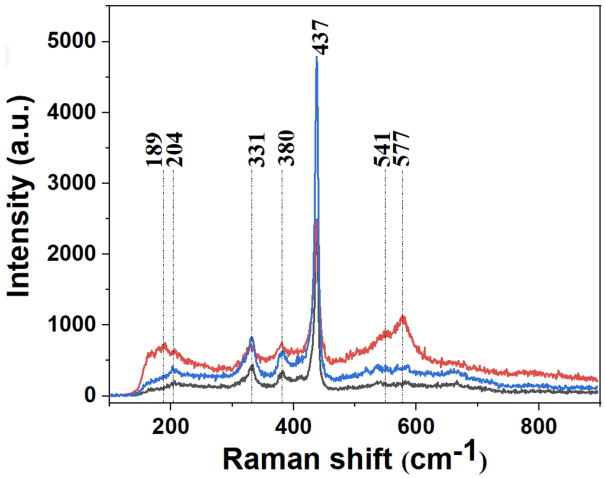

Figure 3.9 Raman spectra of different ZnO films ground (EG solvent) and unground, black (bulk sample), blue (ground at 200 rpm for 10 minutes), red (ground at 750 rpm for 90 minutes).

In our test, the EDX results of ZnO gas sensor film (Figure 3.10) confirmed the existence of Zn and O elements, with average atomic percentages of 48.05 and 51.95, respectively. The percentage of oxygen content in ground powder may be affected by grinding time and medium (e.g. solvent) [63]. the grinding tank and grinding beads may also be polluted by ball milling [63], but the results do not show that there are obvious elemental impurities in the PBM nanoink studied.

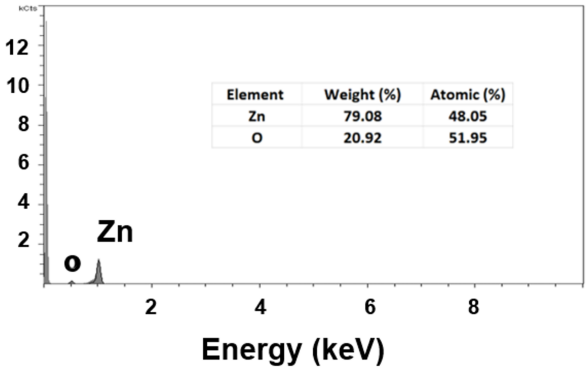

Figure 3.10 EDX spectrum of ZnO film using PBM nanoink ground at 600 rpm for 10 minutes in EG solvent.

3.2 Gas sensor performance and gas sensing properties

3.2.1 Different gases

Figure 3.11 shows current (at +2V bias) vs. time and I-V curves of ZnO thin film sensor formed with EG-400a vials nanoink. After reaching a minimum in the pure dry air flow, a dynamic response is observed, when exposed to the target gas atmosphere. Namely, when the target gas source is injected, the output current increases, and when the gas is released (and re-exposed to dry air/oxygen), the output current decreases. Therefore, the resistance of the sensor decreases as it is exposed to the target and increases as dry air is introduced. In this figure, we can find the relationship between current level and time of dry air/pure argon/dry air flow sequence (similar behavior is observed in nitrogen target gas environment).

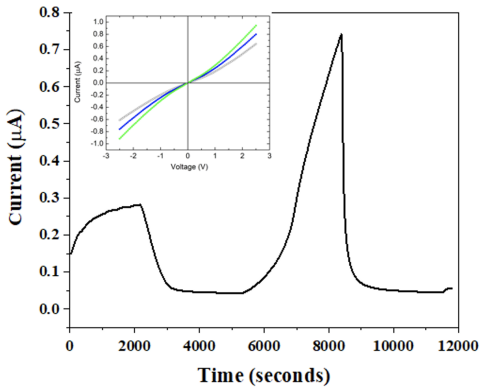

Figure 3.11 Time dependence of sensor current upon exposure to dry air (~ 2000 sec. mark) followed by pure argon gas (~ 5500 sec. mark) and back (~ 8000 sec. mark) (all flows 500 sccm) for ZnO thin film sensors formed using PBM nanoinks ground for 10 minutes in EG (400 rpm). Inset shows I-V plots as current increases near the start of argon flow.

In order to study the stability and repeatability, we have repeated testing our gas sensor under multiple flow sequences. From the Figure 3.12, the target gas response of our sensor can be repeated on multiple flow sequences, but due to the size of the test quartz chamber and the maximum flow rate used (except film thickness), it takes some time to reach the stable baseline, and the figure also shows the sensor is stable after about 2.5 hours. Inset figure shows the current vs. time plot graph for ZnO thin film gas sensors, the target gas response can be repeated over multiple flow sequences of several "on/off" dry air/target gas pulses.

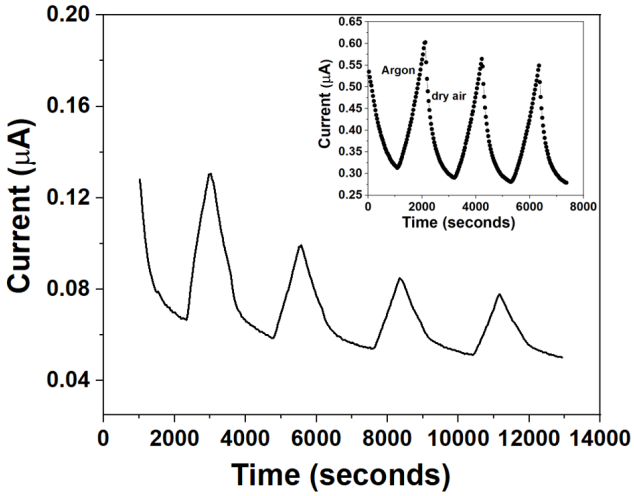

Figure 3.12 Gas sensor (prepared using nanoinks ground at 400 rpm for 10 min in EG solvent) showing approach to stable baseline vs. time during repeated exposure to 250 sccm of H2 pulses. Inset shows sensor current vs. time for a similar sequence of on/off dry air/argon gas pulses for ZnO thin film sensor formed using PBM nanoinks ground for 10 minutes in EG (600 rpm)

Figure 3.13 shows the detection of hydrogen target gas mixed with dry air carrier gas. In here, the current starts to decrease when we put the hydrogen gas balanced with the dry air, and dry air can also be used as the carrier gas for sensing to balance the target carrier.

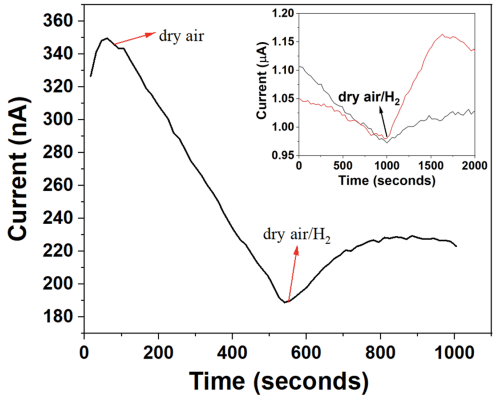

Figure 3.13 Sensor current vs. time for 500 sccm dry air followed by 400 sccm dry air/100 sccm hydrogen for ZnO thin film sensors formed using PBM nanoinks ground for 10 minutes in EG

(600 rpm). Inset shows current vs. time for ZnO sensor in (a) exposed to 450 sccm dry air/50 sccm hydrogen (red curve) and 475 sccm dry air/25 sccm hydrogen (black curve).

3.2.2 Different Humidity

It is observed that, the sample current of the sensor increases (in the ambient atmosphere) while decreases after the introduction to dry air, which indicates that the response of the ZnO Gas thin film sensor is also strongly dependent on the humidity or relative humidity of the working atmosphere. The humidity sensitivity of our ZnO film is confirmed by the data shown in Figure 3.14, which shows a large sensor response compared with the relative humidity. Figure 3.15 shows the I-V measurement

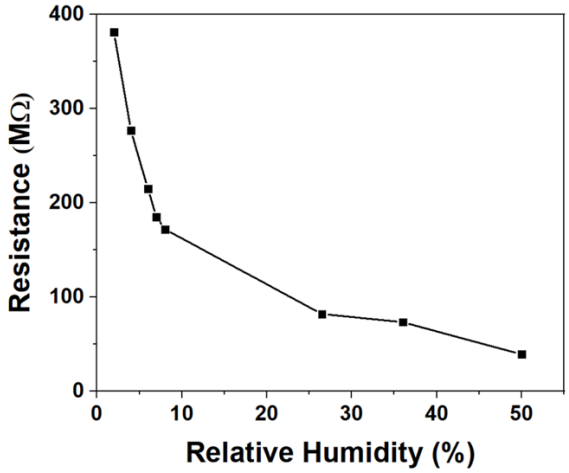

Figure 3.14 Change in resistance at different RH of ZnO gas sensor sample formed using PBM nanoinks ground at 200 rpm for 30 minutes in DI water.

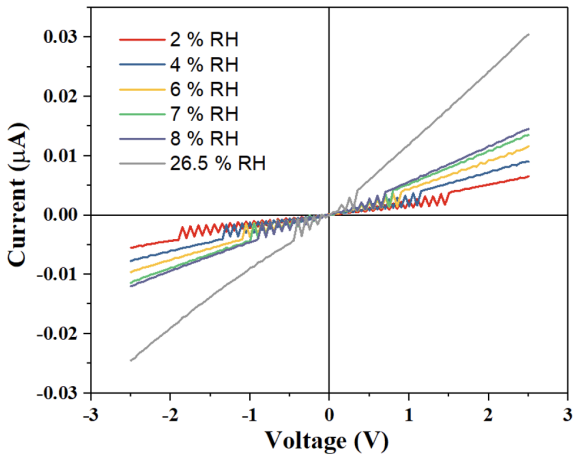

Figure 3.15 I-V measurement of ZnO gas sensor samples formed using PBM nanoinks ground at 200 rpm for 30 minutes in DI water at different RH.

3.2.3 Different Particle Size

Gas sensing response is defined as the ratio of resistance in two different gas environments. In order to compare the performance of thin film gas sensors, which prepared with PBM nanoink under different grinding conditions, the sensor response [73, 74] is calculated as follows (equation 1):

$$S = \frac{R_a - R_g}{R_a} \quad (1)$$

where R_a and R_g are the sensor resistance in dry air and in the presence of target gas, respectively.

Fig. 3.16 and Fig 3.17 compares the effects of different grinding parameters (speed/time/solvent), which on the response of the gas sensor in the presence of argon target gas. We can find out, from Figure 3.16 when the grinding speed exceeds 400 rpm, the sensor response decreases, which may be due to particle agglomeration and porosity change. With the extension of grinding time, the response also increases. When it is reaching a peak in about 30 minutes at a

constant grinding speed of 200 rpm (Figure 3.17), the use of high-energy ball milling abrasive materials will produce surface and large defects. Surface defects may improve gas sensing performance by exposing adsorption sites, while volume defects may limit adsorption area [63]. The Raman data in Figures 3.8 and 3.9 show that with the increase of grinding, surface defects such as Zni - and VO related defects exist. It may lead to a significant increase in the response of the gas sensor, due to more oxygen molecules are easily absorbed and ionized on the ZnO surface [75]. However, long grinding at high speed / time will also produce large defects, so it is expected that large defects will appear in the grinding process, resulting in low response.

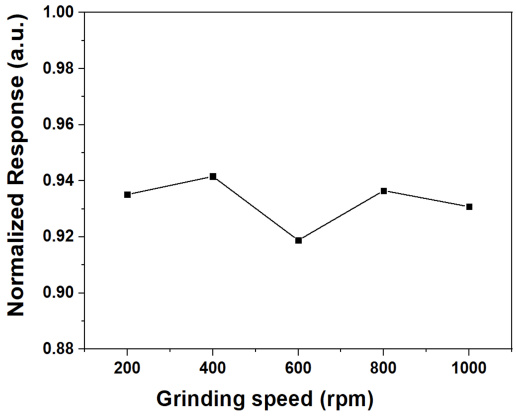

Figure 3.16 Response of different gas sensors made from ground PBM ZnO nanoinks. Films prepared using EG solvent at different grinding speeds for a constant grinding time of 10 minutes.

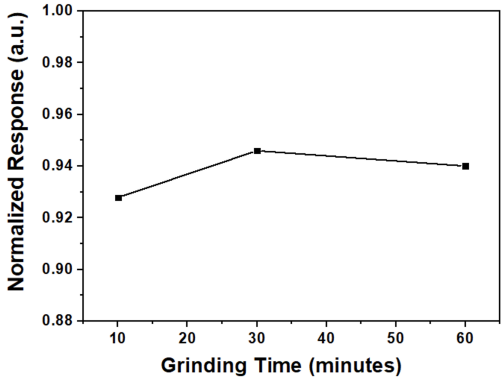

Figure 3.17 Response of different gas sensors made from ground PBM ZnO nanoinks. Films prepared using DI water solvent at different grinding times for a constant grinding speed of 200 rpm.

3.2.4. Different Temperatures

To further explore the performance of the gas sensor, we studied the effect of operating temperature on the sensor response: the thermal activation process will affect the reaction mechanism, carrier concentration and mobility on/near the sensing surface, all of these will affect the detection response and dynamic behavior of the gas sensor [76]. Figure 3.18 shows the temperature related sensor response data, indicating the best operation near 100 ℃ and others decreasing, when there is higher temperature, which is consistent with the previous work using metal oxides [77]. Similarly, the shortening of response and recovery time at high temperature (Figure 3.19) is due to the reduction of activation energy required for surface reaction, that is, faster absorption and desorption occur on the zinc oxide surface, thus shortening the response/recovery time [50].

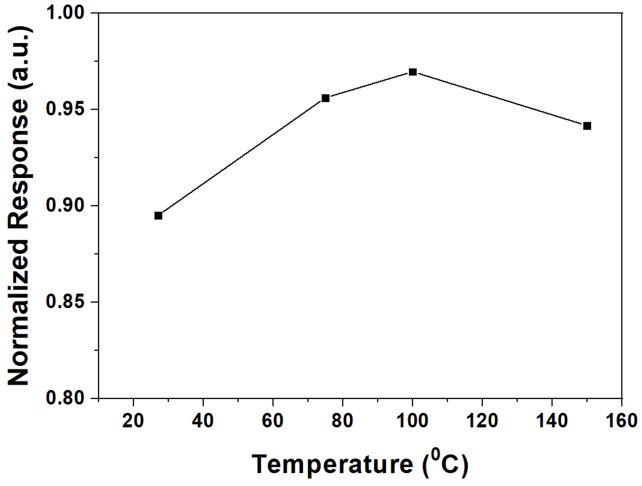

Figure 3.18 Normalized response for sensors prepared from ZnO nanoinks ground at 600 rpm for 10 minutes using EG solvent.

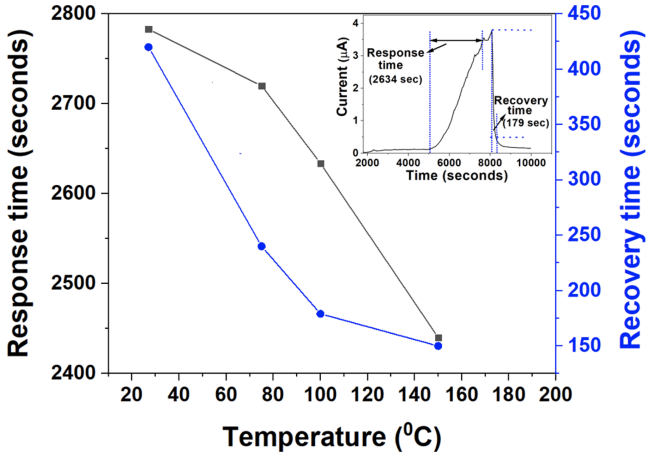

Figure 3.19 Response and recovery time. The inset shows the time dependence of sensor current upon exposure to dry air followed by argon test gas at 100 C.

3.2.5 Limit of Detection (LOD) and Selectivity

The sensor response was further studied for limit of detection. In most of articles, the limit of detection is defined by testing the gas sensor with the lowest concentration of the target gases (1 ppm) [78, 79]. However, some articles also tried to calculate the optimized LOD value by following procedures. Demontis et al. [80] have plot the figure and showed baseline resistance (R_{air}/R_0) normalized to one, and reported the sensor resistance in gas (R_{gas}/R_0). They summed three times of the noise of the baseline resistance to the value of normalized baseline value, and got the horizontal line at 1.3, the LOD (3ppm) has been calculated from the intercept between this line and the extrapolation fit of the data for each specific analyte. In our measurement, a range of hydrogen concentrations in the range of 5000 to 20000 ppm due to the limitation of the experiment equipment. Figure 3.20 shows the thin film sensor sample that prepared using PBM nanoinks

ground at 400 rpm for 10 minutes with EG solvent from 5000 to 20000 ppm concentration of H_2 gas. The inset figure showed a linear response region with a sensitivity of about $2.4x10^{-2}$ ppm^{-1}.

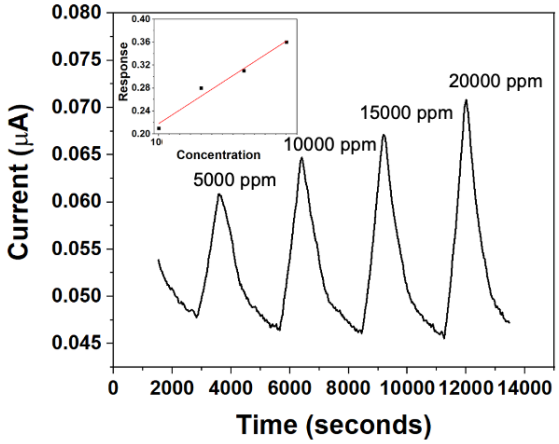

Figure 3.20. Current vs. time for ZnO thin film sensor (prepared using PBM nanoinks ground at 400 rpm for 10 minutes in EG solvent) at different H2 gas concentrations indicated. Inset shows response as a function of gas concentration.

And again, the selectivity of the sensor was tested by exposing different gas species (Fig. 3 (f)) to the same concentration and showed a strong response to methane, followed by hydrogen and argon, which showed the potential of selective gas sensing (Fig. 3 (f), illustration). Preferential adsorption of different gas molecules [81] may lead to the sensor selectivity observed at room temperature. When cycling back to the first gas pulse (H2), the original sensor signal returns.

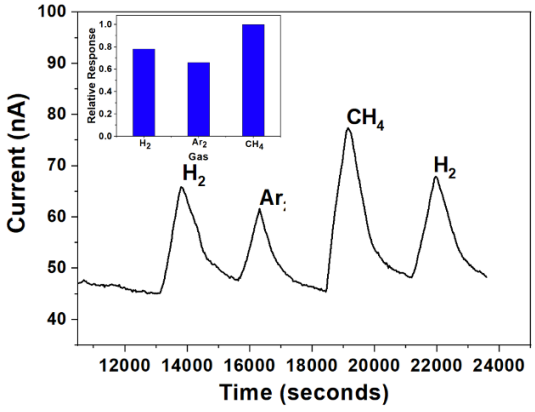

Figure 3.21. Current vs. time for ZnO thin film sensor when exposed to different gases (hydrogen, argon and methane). Inset shows relative response or selectivity to different target gas species.

3.3 Discussion and Analysis

3.3.1 Recovery Time and Response Time

The key characteristic of sensor performance is the response/recovery time of the sensor. Response time is usually defined as the time required for the sensor to achieve 90% of the total signal response (such as resistance) when exposed to the target gas [73]. Recovery time is usually defined as the time required for the sensor to recover to less than 10% of the original signal after removing the target gas [73]. The response and recovery time depend on the diffusion path (the distance of gas passing through the pores of the nanoparticle sensing surface), the film porosity and particle agglomeration [82-84]. According to the results in Figure 3.22 (a), compared with the sensor prepared from the higher grinding speed, the gas sensor prepared from the PBM nanoink with lower grinding speed has faster response, the response time reaches the maximum value, close to 600 rpm, and then decreases again at the higher speed. Meanwhile, increasing the grinding time seems to increase the response time, and a horizontal offset of nearly 30 minutes is observed (Figure 3.22 (c)). The recovery time of the gas sensor usually increases to 600 rpm with the grinding speed, and then decreases at 800 RPM (Figure 3.22 (b)), while the grinding time of about 30 minutes also shows a decrease (Figure 3.22 (d)), indicating that the recovery speed of the sensor is faster. In general, in order to have an effective sensor that capable of rapid response/recovery, the best combination of nanoink grinding conditions should be selected. According to Figure 3.20, it seems to occur at low to medium grinding speed (200-400 rpm) and medium grinding time

(about 30 minutes), and even possibly higher grinding speed (about 800 rpm) and short grinding time (about 10 minutes) of the equipment under study.

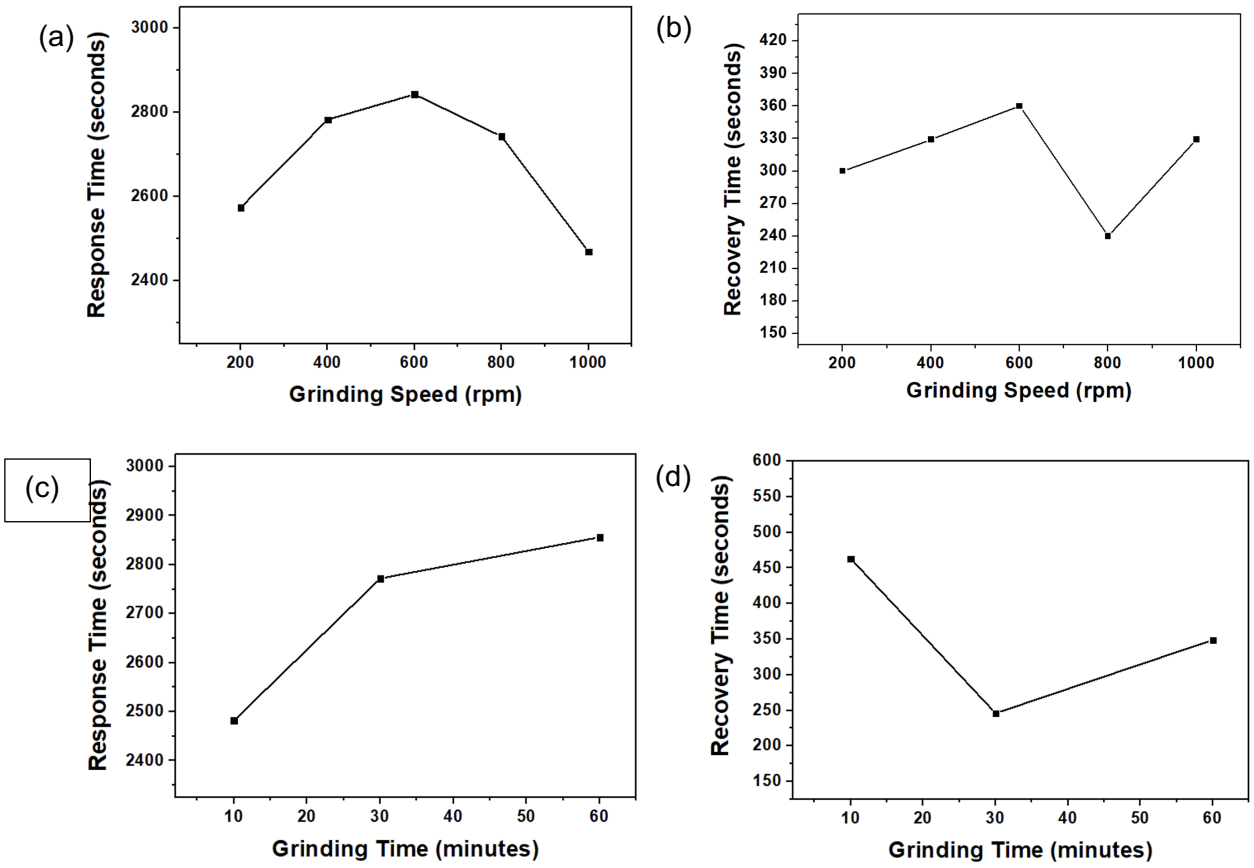

Figure 3.22 Response time (a) and recovery time (b) of sensors prepared from ZnO nanoinks ground at different speeds for constant grinding time of 10 minutes using EG solvent. Response time (c) and recovery time (d) of sensors prepared from ZnO nanoinks ground at constant speed of 200 rpm for different grinding times using DI water solvent.

3.3.2 Operating Temperature

In general, the gas sensing characteristics of metal oxide semiconductor (MOS) gas sensor materials are related to surface chemical reaction and gas diffusion. As a typical n-type MOS sensor, the conductivity of ZnO based sensor is affected by gas interaction, and gas adsorption is

related to the material surface. At lower temperature (< 150 ℃), the surface chemical reaction plays a leading role and will be very slow. The adsorbed oxygen can only capture a small number of electrons to form O_{2ads}^-. Therefore, the larger specific surface area of the material provides more active sites and higher sensitivity. When the temperature is over 150 °C but less than 300 °C, surface chemical reaction and gas diffusion produce common manipulation effects. When the temperature exceeds 300 °C, O_{2ads}^- continues to capture electrons to form electrons O_{ads}^- and O_{ads}^{2-}. Therefore, the surface chemical reaction accelerates, and the gas diffusion becomes the speed limiting step. In this case, with the more larger pore size and porosity of the material existed, the more favorable in gas diffusion and the enhanced gas sensitivity are showed. The process of adsorbing oxygen ions can be described by the following equation (eq. (2)-(5)) [85]:

$$O_{2gas} \leftrightarrow O_{2ads} \quad (2)$$

$$O_{2ads} + e^- \leftrightarrow O_{2ads}^- \ (T \leq 150\ ℃) \quad (3)$$

$$O_{2ads}^- + e^- \leftrightarrow 2O_{ads}^- \ (150\ ℃ \leq T \leq 300\ ℃) \quad (4)$$

$$O_{ads}^- + e^- \leftrightarrow O_{ads}^{2-} \ (T \geq 300℃) \quad (5)$$

3.3.3 Mechanism

The response of a thin film gas sensor is related to particle size and porosity. The factors which affecting pore size are particle size, separation performance and particle arrangement. When the separation is well enough, the larger particle led to the larger pore. When it is poor, the pore size depends on the diameter of small particles, due to the pores formed by coarse particles are filled by small particles. Figure 3.1 (b) shows that powders milled at higher speeds tend to obtain smaller particle sizes. The smaller the particle size, the larger total surface area is. The improvement of sensor performance is proportional to the decrease of particle size [84]. This

supports the increase in normalized sensor response when the grinding speed approaches 400 rpm and the grinding time reaches 30 minutes. With the further decrease of particle size (< 200 nm), the nanoparticles may agglomerate, thus reducing the effective surface area and free surface energy [86] (in addition, the large particle size dispersion in the 600 rpm sample in Figure 3.5 may exacerbate this effect). The effect of caking is consistent with the reduction of porosity of samples made by grinding nanoink at higher speed (see Figure 3.23 (a)) [52]. The lower porosity can also explain the faster response/recovery time of some samples which observed in Figure 3.22. According to the material characteristic data, grinding ZnO materials will eventually lead to the increase of surface and bulk defects. Generally, the defect density on the surface is higher than that in the block [87]. Surface defects act as (I) charge carrier traps and (II) adsorption sites to improve electron hole separation [88]. On the other hand, bulk defects act as rebinding sites [89]. Therefore, the effect of grinding on gas sensing behavior depends on the ratio of bulk defects to surface defects. Initially, with the increase of grinding time/speed, the ratio of volume defects to surface defects decreases, which can be attributed to the relatively high surface defects caused by the increase of total surface area. However, according to our results at higher grinding speed and time, this ratio seems to increase due to the formation of excessive bulk defects, which may be attributed to the deformation of bulk crystals caused by excessive mechanical wear.

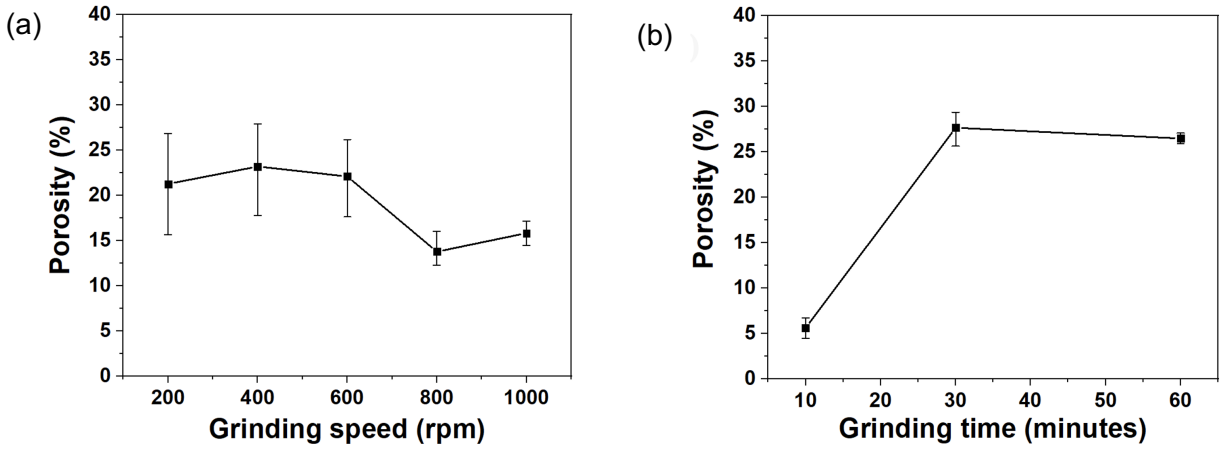

Figure 3.23 Change in porosity of sensors prepared using ZnO nanoinks. (a) Sensor prepared using EG solvent for different grinding speeds at constant grinding time of 10 minutes. (b) Sensor prepared from DI water solvent at different grinding times for constant grinding speed of 200 rpm.

ZnO is a surface sensitive material, when it is used to prepare sensing elements, the gas sensing mechanism can be summarized as adsorption oxidation desorption. and the gas sensing mechanism is shown in Figure 3.24 [90]. The sensing mechanism in our sensor may depend on the surface interaction and charge transfer between adsorbed gas species, resulting in the change of sensor resistance (or conductivity) [91]: In air, oxygen molecules are adsorbed on the surface of zinc oxide materials, and electrons are trapped from the conduction band of zinc oxide to form oxygen anion (O^{-2} , O^{-} , O_2^{-}), which becomes the surface acceptor state. Due to the electron loss in the conduction band, a high barrier electron depletion region is formed on the surface of ZnO, which hinders the movement of electrons between grains. Between grains, the combination of two depletion regions produces Schottky barrier, which determines the conductivity of the material [52]. The reaction between the adsorbed oxygen species and the adsorbed gas molecules can change the strength of the Schottky barrier, resulting in the change of the resistivity of the sensor: in the dark, when the zinc oxide surface is exposed to the air environment, the electrons from the

ZnO conduction band ionize the oxygen in the atmosphere, and produce negative oxygen ions (eq. (2)) on the surface of the nanostructured film, thus forming a negative oxygen ion near the surface Low conductivity depletion layer [92].

$$O_2(gas) + e^- \rightarrow O_2^-(ads) \qquad (2)$$

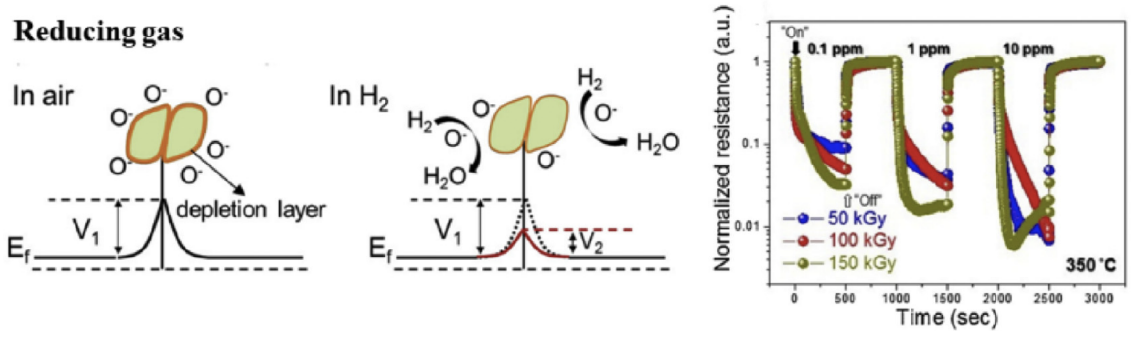

Figure 3.24 The schematic illustration of gas sensing mechanism of ZnO. Oxygen species will absorb electrons in air, grain boundaries will become a potential barrier for electron flow. In H_2, due to the metallization of ZnO, the potential barrier almost disappears, resulting in a significant reduction in the sensor resistance. [93]

When the incident energy is larger than the bandgap of ZnO, the electron hole pairs will be generated. The holes generated by optical absorption migrate to the surface along the potential slope generated by band bending, neutralize the negatively charged adsorbed oxygen ions (eq. (3)), and then desorb, while the photogenerated electrons reduce the width of the depletion layer, thus increasing the conductivity [92].

$$h^+ + O_2^-(ads) \rightarrow O_2(gas) \qquad (3)$$

Therefore, the dark conductivity and photoconductivity of our ZnO films are strongly dependent on the ambient gas conditions and oxidation atmosphere. In addition, relative humidity (defined as the amount of water vapor in the air, expressed as the percentage of the maximum amount that the air can maintain at a given temperature) can also affect the metal oxide surface strongly [94], thereby changing the sensor response [95]. Water molecules adsorbed on the surface tend to dope ZnO with electrons and/or replace the previously adsorbed ionized oxygen to release electrons back to the conduction band (i.e., contrary to eq. (2)) [96]. In both cases, the conductivity of the sensor increases.

3.4 Summary

In this report, we fabricated a chemiresistive ZnO thin-film gas sensor that works at room temperature by using PBM nanoinks and doctor blading method, which can be used to detected the gas type effectively,（dry air/oxygen, argon, nitrogen, hydrogen, methane and atmospheric humidity. ZnO nanoink is prepared by the PBM method, in this way, the particle size of zinc oxide can be controlled by controlling the grinding speed and grinding time, as well as optimize the nanoparticle structure and electrical properties of the obtained film, to realize high-efficiency gas sensing. In this chapter, we have studied the film morphology and material characterization through the roughness, photoluminescence spectrum, Raman spectra, and EDX results. We also analyzed the gas sensing performance of thin film gas sensor samples with different grinding speed and grinding time from the measured I-V data and current and time data. Some parameters may affect the response of the sample, such as operating temperature, relative humidity, light conditions, concentration of testing gas and different gases. For operating temperature (as shown in Figure

3.18), the sensor response increasing when the temperature increasing until reach the operating temperature (nearly 100ºC). For relative humidity (as shown in Figure 3.14), the current seems increasing when the RH is increase (from 2% to 50%). For concentration of testing gas (as shown in Figure 3.20), the sensor response will decrease when the gas concentration is dropping from 20000 ppm to 5000 ppm and showed a linear response region (Figure 3.20 inset) with a sensitivity of approximately $2.4x10^{-2}$ ppm^{-1}. Table 3.1 below summarizes data for ZnO gas sensors fabricated, by using different synthesis techniques, to compare the response to different gas species to our result under 5000 ppm hydrogen gas. From the table, the differentiation with our gas sensor other works fabricate by using ball milling methods, such as CuO coated ZnO, SnO_2 doped ZnO, and ZnO-CuO composite, is that others require to operating at high temperatures range between 180 - 450 ºC, but our gas sensor can present a better gas response under room temperature. For different gases (Figure 3.21), which shows a strong response to methane. We have controlled these parameters and tested under ambient light conditions, room temperature and stable relative humidity. The final properties may depend on the grain size, porosity, and surface volume defect ratio in the film. The porosity results (Figure 3.23) show that the sensor based on PBM nanoink has a high specific surface area, reaches a peak near the grinding speed of 400 rpm, and finally produces more active centers and gas diffusion channels. Overall, the sensor signal magnitude and response/recovery time are improved by changing milling speed and time of the ZnO nanoinks and found that the nanoinks milled at 400 rpm and 30 minutes reaches the best performance.

Table 3.1 Brief summary of gas sensor response for ZnO-based devices operating at different temperatures.

Material	**Target gas**	**LOD**	**Response /Temperature**	**Response time/**	**Ref**

				Recovery time	
Present work	H_2 (5000 ppm)	500 ppm	21%[b]/ RT	-	-
CuO coated ZnO using ball milling method	H_2 (200 ppm)	-	~15[a]/ 300 ^{0}C	-	[81]
ZnO nanotube using chemical etching process	H_2 (500 ppm)	5 ppm	~29.6%[b]/ RT	~540 s/-	[82]
SnO_2 doped ZnO using ball milling method	CO (200 ppm)	-	~5[a]/ 450 ^{0}C	-	[83]
ZnO- CuO composite via ball milling process	CO (200 ppm)	-	~12.2[a]/ 180 ^{0}C	-	[84]
Pt-doped ZnO using RF sputtering	H_2 (1000 ppm)	250 ppm	~5.5[a]/ 200 ^{0}C	36 s/112 s	[85]
ZnO nanowires by thermal evaporation	H_2 (100 ppm)	50 ppm	~5.5[a]/ 200 ^{0}C	30 s/-	[86]

[a)] $S = R_a/R_g = I_g/I_a$ [b)] $S = (R_a-R_g)/R_a*100\%$

Chapter 4

Conclusion

4.1 Future Work

In recent years, due to the higher demands and standards for the accuracy, selectivity, sensitivity, and stability of gas sensors in the fields of industrial production, family safety, environmental monitoring and medical treatment, the future research and development of gas sensors are more imperative. With the miniaturization, intelligence, and multi-function of gas sensors, the preparation and application of ZnO nanomaterials will have significantly developed. Due to the excellent properties of nanomaterials and the advantages of the usage of gas sensing materials, the application of nanomaterials can improve the stability of the traditional gas sensor. However, future research and development methods, which can better improve the gas sensing performance through effective control of structure and morphology, as well as through element doping modification in synthetic gas sensing materials, should be considered as a key problem since it limits the research and development in this field. Due to the whole project focusing more on the ZnO thin film gas sensor based on the PBM method, several approaches for further research in this study field will be advanced.

4.1.1 Device fabrication and structures

Up to the present, scientists already successfully prepared ZnO nanomaterials with various morphologies and structures, which involved one-dimensional ZnO nanomaterials, such as ZnO nanoparticles, nanowires, nanobelts, nanorods, nanocables, and porous ZnO nanostructures. The

synthesis methods include physical and chemical methods, such as spray pyrolysis, physical vapour deposition, chemical vapour deposition, hydrothermal method, and microwave pyrolysis [85]. Every single method can synthesize high-quality nanostructures and apply them to gas sensors. One-dimensional material is characterized by large specific surface area, slow electron breakdown rate, and various surface morphologies. Two-dimensional materials have significant carrier transportability, high gas permeability, and high active surface exposure rate. And three-dimensional materials have high porosity and large specific surface area, which can effectively promote the adsorption and diffusion of a gas. Therefore, with superiority, three-dimensional materials with hollow, mesoporous, and core-shell structures have become the research focus in fields of study [85]. In this report, we only present the test with ZnO thin film gas sensor, which applied two-dimensional materials using PBM fabrication method and changed the different grinding conditions, such as the grinding speed (from 200 - 1000 rpm), grinding time (10 min - 60 min) and grinding solvent. In future studies, we suggested trying to improve the grinding time to a much longer time (such as to 10 hours if possible) and compare the results. And we also suggest developing some one-dimensional or three-dimensional materials, as well as other possible fabrication methods to test the gas sensitivities.

4.1.2 Composite and Dopant Materials

Pure ZnO gas sensors have been also proved with disadvantages of low sensitivity, high working temperature, and poor selectivity. Thus, for the further improvement of gas sensing performance, element doping is needed. Dopants can be applied to provide surface-active points and preferentially adsorb and target gas molecules, while gas sensing reaction. The adsorbed target

molecules combine with the semiconductor surface to change its conductivity, which will achieve the detection of target gas molecules. To summarize the above research results, element doping is an important method to improve the selectivity and response speed of semiconductor gas sensors.

There are also several aspects that dopants' researchers can be expanded for improving gas sensor sensitivities: (1) precious metals: at present, the main precious metal elements doped in ZnO semiconductors are as follows: Pd, Ag, Ru, Au, etc. (2) Rare earth elements: the common rare earth oxides used for doping are as follows: CeO_2, Ia_2O_3, Y_2O_3, etc. (3) Metal oxides: Since metal oxides will not appear as a poisoning phenomenon, with the bargain price, oxides have been widely concerned by researchers, which have commonly used for doping are TiO_2, In_2O_3, SnO_2, etc. Instead of element doping, combining zinc oxide with other materials is also a common method. In addition, different materials can be combined to form heterojunctions, homojunction, and Schottky junctions, which are beneficial to reduce the grain boundary barrier and facilitate electron migration within the materials [97]. Furthermore, there is a synergistic effect between different components in the composite, which can constantly improve the gas sensing performance of the matrix material [98]. Frequently, in order to enhance gas sensing properties, ZnO is generally combined with heteroelements (such as Pt, Pd, Au, Mn, In, etc.) Metal oxide (such as In_2O_3 and CuO.) Conductive polymers (such as polyaniline, polythiophene, polypyrrole, etc.) Carbon materials, two-dimensional materials such as GaN, SiC, g-C_3N_4, graphene, and its derivatives. Drmosh al et. [99] studied the H2 gCas sensing properties of Au nanoparticles decorated rGO/ZnO heterostructure and investigated the sensor properties at RT under UV irradiation. They have prepared their studies with three different types of gas sensors (a) ZnO nanorods, (b) rGO/ZnO heterostructure, and (c) Au decorated rGO/ZnO.

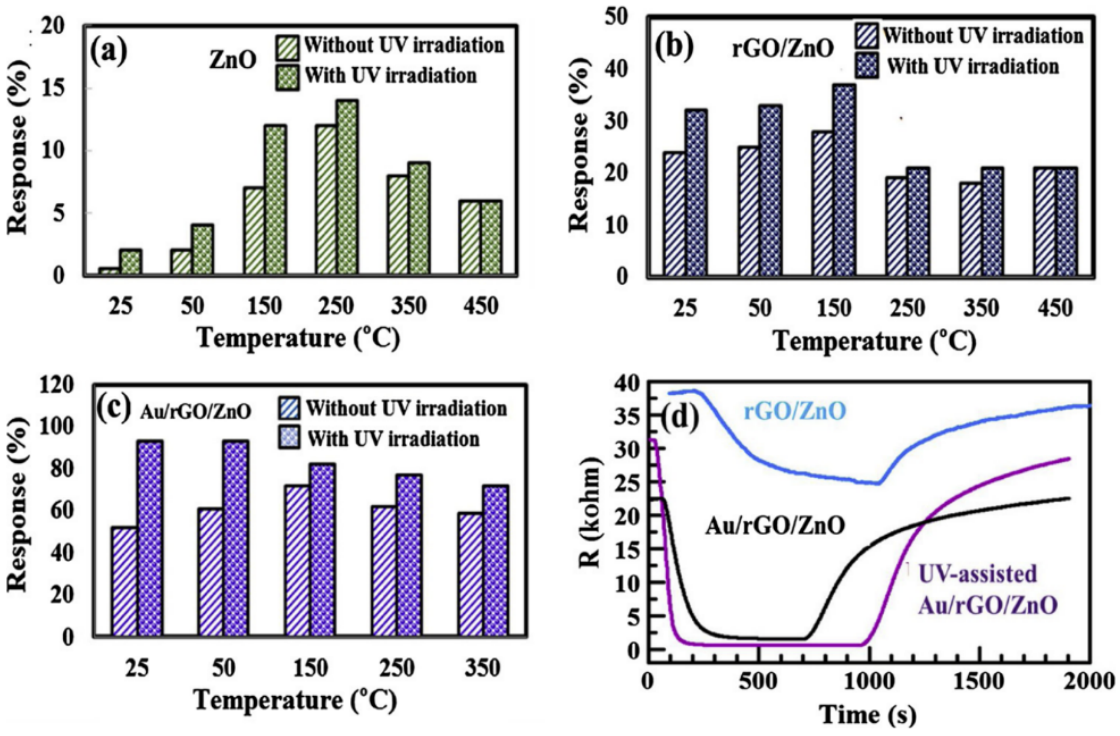

Figure 4.1 (a)–(c) Comparison of the response of pristine ZnO, rGO/ZnO, and Au/rGO/ZnO sensor with and without UV irradiation at different operating temperatures, and (d) dynamic response of rGO, Au/rGO/ZnO, and UV activated Au/rGO/ZnO at RT. [99]

Above all, this report only summarized our study of the gas sensor properties for pure ZnO thin film. In the future study, we recommend trying to prepare some gas sensor samples doped or combined with other metal elements to test and compare the response of gases.

4.1.3 Other Improvements

Our studies are mainly focusing on the testing of the gas sensor properties of our ZnO thin film sensor by using PBM nanoinks, and we have tested the gas sensor properties widely, such as operating temperature, relative humidity, the limit of detection and selectivity, etc.

However, due to the limitation of our gas sources, measure system, and gas sensor sample preparation process, we haven't gotten a chance to test deeply. Therefore, we concluded three factors, which can be improved in future tests, in order to get more data for gaining in-depth knowledge and study. Firstly, for gas sensor thickness, we only use one type of the scotch tape to control the thickness (approximately 60 μm). For future research, we could use different layers of the scotch tapes with different thickness to create different thickness gas sensor samples for further measurement. Secondly, for the limit of detection, we finally tested our sensor only under H_2 with a concentration from 5000 ppm - 20000 ppm. We believe that the upgrading of the measuring system, such as making a smaller chamber and putting an additional mixing chamber, as well as measures with lower concentration, will be supportive to solve the limit of detection limitation problem (lower to 10 ppm). Finally, for the selectivity, we have tested the sensor under 3 different test gases, hydrogen, argon, and methane. We can also broaden the test with different gas sources, such as CO, NO_2, NH_3, etc.

4.2 Summary

To conclude the above research results and our studies' outcomes, with the rapidly growing demand for production and human living conditions, the high working temperature of traditional electrochemical gas sensors cannot meet the needs of the current increasingly complex work environment. Since the ZnO-based gas sensors, as a promising room-temperature sensing material, have been widely concerned and studied, the development of the ZnO-based gas sensors has become a major research topic in the field, which can help develop efficient and energy-saving gas sensors working at room temperature.

This report has been present the overall objective of our studies and tests were to explore the gas sensitivity of ZnO thin films formed via nano-grinding using PBM, which has been indicated as a relatively cheap, reliable, direct, repeatable, and adjustable method to reduce the particle size of powder materials. As mentioned in the introduction part, hydrogen gas has gained remarkable attention. Table 4.1 below shows the advantages and disadvantages of other competitive sensors for hydrogen gas sensors with different materials. It indicated the fabricated costs of semiconductor metal oxide (such as ZnO, the tested material in this report) gas sensors and carbon-based (such as CNTs and graphenes) gas sensors are competitive. In addition, those materials not only have a high response with a sufficient limit of detection but also have the capability of thermal and chemical stability. Although the metal-based gas sensor (such as Pd-based) can detect H_2 with high selectivity operating at room temperature, the sensing has underperformed to a low concentration of H_2, with an unsatisfactory response and recovery times, with higher costs. There are certainly some disadvantages to the semiconductor metal oxide gas sensors, including high power consumption, high operating temperature, poor selectivity, and vulnerability to humidity. Therefore, further research and tests are needed to work on the weakness of the materials.

Sensor	Material	Mechanism	Advantages	Disadvantages
Metal based	Pd	• Phase transition • Decrease resistance by volume expansion	• RT operation • High selectivity • Faster response • High thermal/chemical stability	• Poor sensing to low concentration • Poor durability • Expensive
SMO	ZnO	• Chemisorption reaction • Metallization of MO oxide	• Microporous structure • High response • Low detection limit	• High operating temperature • High power consumption

			• High thermal/chemical stability • Low fabrication cost	• Poor selectivity • Vulnerability to humidity
Carbon based	Pd/CNTs	Phase transition process Schottky barrier modulation	• Operation at RT • High surface area • Low fabrication cost	• Limited strategies for the sensor fabrication • Poor selectivity • Poor reproducibility • Vulnerability to humidity

Table 4.1 other competitive material [100]

Chapter 2 provides the discussion of the grinding process and parameters, as well as the preparation and measurement system set up of the films. Chapter 3 gives the outcomes of resistive ZnO thin film gas sensors, that can be fabricated using PBM nanoink and doctor blade, to create active sensor materials, which can work effectively at room temperature, to detect changes in dry air/oxygen, argon, nitrogen, and hydrogen species, and atmospheric humidity. We finalized that by changing the grinding parameters, the film is composed of ZnO nanoparticles with adjustable size and porosity. As well as the response of different gas sensors to grinding speed shows that the nanostructured film made of ZnO nanoink grinded at 400 rpm produces the best combination of sensor signal amplitude and dynamic behavior (time response). The last part of this report includes our reflection of our studies and tests, proposes the future research and development directions, and discusses potential application prospects.

References

[1] S. Bayda, M. Adeel, T. Tuccinardi, M. Cordani, and F. Rizzolio, "The history of nanoscience and nanotechnology: from chemical–physical applications to nanomedicine," *Molecules,* vol. 25, no. 1, p. 112, 2020.

[2] J. Jeevanandam, A. Barhoum, Y. S. Chan, A. Dufresne, and M. K. Danquah, "Review on nanoparticles and nanostructured materials: history, sources, toxicity and regulations," *Beilstein journal of nanotechnology,* vol. 9, no. 1, pp. 1050-1074, 2018.

[3] M. T. Bohr, "Nanotechnology goals and challenges for electronic applications," *IEEE Transactions on Nanotechnology,* vol. 1, no. 1, pp. 56-62, 2002.

[4] D. Guidance, "Considering Whether an FDA-Regulated Product Involves the Application of Nanotechnology," ed: FDA, 2011.

[5] Y.-F. Sun *et al.*, "Metal oxide nanostructures and their gas sensing properties: a review," *Sensors,* vol. 12, no. 3, pp. 2610-2631, 2012.

[6] H. C. Zeng, "Synthetic architecture of interior space for inorganic nanostructures," *Journal of Materials Chemistry,* vol. 16, no. 7, pp. 649-662, 2006.

[7] M. N. F. Norrrahim *et al.*, "Nanocellulose: the next super versatile material for the military," *Materials Advances,* 2021.

[8] A. Rae, "Real life applications of nanotechnology in electronics," *OnBoard Technol,* vol. 2006, p. 28, 2006.

[9] G. E. Moore, "Cramming more components onto integrated circuits," ed: McGraw-Hill New York, 1965.

[10] G. E. Moore, "Progress in digital integrated electronics," in *Electron devices meeting*, 1975, vol. 21: Washington, DC, pp. 11-13.

[11] K. König and A. Ostendorf, "Optically induced nanostructures: biomedical and technical applications," 2015.

[12] G. Mothé *et al.*, "Detection of greenhouse gas precursors from diesel engines using electrochemical and photoacoustic sensors," *Sensors,* vol. 10, no. 11, pp. 9726-9741, 2010.

[13] K. Suematsu *et al.*, "Nanoparticle cluster gas sensor: controlled clustering of SnO2 nanoparticles for highly sensitive toluene detection," *ACS applied materials & interfaces,* vol. 6, no. 7, pp. 5319-5326, 2014.

[14] K. Suematsu, K. Watanabe, A. Tou, Y. Sun, and K. Shimanoe, "Ultraselective toluene-gas sensor: nanosized gold loaded on zinc oxide nanoparticles," *Analytical chemistry,* vol. 90, no. 3, pp. 1959-1966, 2018.

[15] Q. T. H. Ta, G. Namgung, and J.-S. Noh, "Synthesis of Ag@ rGO/gC 3 N 4 Layered Structures and Their Application to Toxic Gas Sensors: Effect of Ag Nanoparticles," *Electronic Materials Letters,* vol. 15, no. 6, pp. 750-759, 2019.

[16] M. Mhadhbi, "Modelling of the High-Energy Ball Milling Process," *Advances in Materials Physics and Chemistry,* vol. 11, no. 1, pp. 31-44, 2021.

[17] Z. Zhu, Y. Xu, and B. Jiang, "A one ppm NDIR methane gas sensor with single frequency filter denoising algorithm," *Sensors,* vol. 12, no. 9, pp. 12729-12740, 2012.

[18] H. Nazemi, A. Joseph, J. Park, and A. Emadi, "Advanced micro-and nano-gas sensor technology: A review," *Sensors,* vol. 19, no. 6, p. 1285, 2019.

[19] A. Dey, "Semiconductor metal oxide gas sensors: A review," *Materials Science and Engineering: B,* vol. 229, pp. 206-217, 2018.

[20] S. Amirkhanlou, M. Ketabchi, and N. Parvin, "Nanocrystalline/nanoparticle ZnO synthesized by high energy ball milling process," *Materials letters,* vol. 86, pp. 122-124, 2012.

[21] C. F. Burmeister and A. Kwade, "Process engineering with planetary ball mills," *Chemical Society Reviews,* vol. 42, no. 18, pp. 7660-7667, 2013.

[22] D. S. Kumar, B. J. Kumar, and H. Mahesh, "Quantum nanostructures (QDs): an overview," *Synthesis of Inorganic Nanomaterials,* pp. 59-88, 2018.
[23] H. Mio, J. Kano, F. Saito, and K. Kaneko, "Effects of rotational direction and rotation-to-revolution speed ratio in planetary ball milling," *Materials Science and Engineering: A,* vol. 332, no. 1-2, pp. 75-80, 2002.
[24] D. Zhang, "Processing of advanced materials using high-energy mechanical milling," *Progress in Materials Science,* vol. 49, no. 3-4, pp. 537-560, 2004.
[25] A. V. Rane, K. Kanny, V. Abitha, and S. Thomas, "Methods for synthesis of nanoparticles and fabrication of nanocomposites," in *Synthesis of inorganic nanomaterials*: Elsevier, 2018, pp. 121-139.
[26] D. R. Lide, *CRC handbook of chemistry and physics*. CRC press, 2004.
[27] C. Klingshirn, "ZnO: material, physics and applications," *ChemPhysChem,* vol. 8, no. 6, pp. 782-803, 2007.
[28] C. Klingshirn, "ZnO: From basics towards applications," *physica status solidi (b),* vol. 244, no. 9, pp. 3027-3073, 2007.
[29] Ü. Özgür *et al.*, "A comprehensive review of ZnO materials and devices," *Journal of applied physics,* vol. 98, no. 4, p. 11, 2005.
[30] V. A. Coleman and C. Jagadish, "Basic properties and applications of ZnO," in *Zinc oxide bulk, thin films and nanostructures*: Elsevier, 2006, pp. 1-20.
[31] A. B. Djurišić, X. Chen, Y. H. Leung, and A. M. C. Ng, "ZnO nanostructures: growth, properties and applications," *Journal of Materials Chemistry,* vol. 22, no. 14, pp. 6526-6535, 2012.
[32] W. Gao and Z. Li, "Nanostructures of zinc oxide," *International journal of nanotechnology,* vol. 6, no. 3-4, pp. 245-257, 2009.
[33] X. Shen, P. B. Allen, J. T. Muckerman, J. W. Davenport, and J.-C. Zheng, "Wire versus tube: stability of small one-dimensional ZnO nanostructures," *Nano letters,* vol. 7, no. 8, pp. 2267-2271, 2007.
[34] Z. L. Wang, "Nanostructures of zinc oxide," *Materials today,* vol. 7, no. 6, pp. 26-33, 2004.
[35] Z. L. Wang *et al.*, "Semiconducting and piezoelectric oxide nanostructures induced by polar surfaces," *Advanced Functional Materials,* vol. 14, no. 10, pp. 943-956, 2004.
[36] S. Vyas, "A short review on properties and applications of ZnO based thin film and devices," *Johnson Matthey Technology Review,* 2020.
[37] H. Liu, V. Avrutin, N. Izyumskaya, Ü. Özgür, and H. Morkoç, "Transparent conducting oxides for electrode applications in light emitting and absorbing devices," *Superlattices and Microstructures,* vol. 48, no. 5, pp. 458-484, 2010.
[38] S.-J. Kim, "Improvement of GaN-based light-emitting diode by indium-tin-oxide transparent electrode and vertical electrode," *IEEE Photonics technology letters,* vol. 17, no. 8, pp. 1617-1619, 2005.
[39] H. Agura, A. Suzuki, T. Matsushita, T. Aoki, and M. Okuda, "Low resistivity transparent conducting Al-doped ZnO films prepared by pulsed laser deposition," *Thin solid films,* vol. 445, no. 2, pp. 263-267, 2003.
[40] B.-Z. Dong, G.-J. Fang, J.-F. Wang, W.-J. Guan, and X.-Z. Zhao, "Effect of thickness on structural, electrical, and optical properties of ZnO: Al films deposited by pulsed laser deposition," *Journal of Applied Physics,* vol. 101, no. 3, p. 033713, 2007.
[41] F. Rahman, "Zinc oxide light-emitting diodes: a review," *Optical Engineering,* vol. 58, no. 1, p. 010901, 2019.
[42] S. T. Tan *et al.*, "Blueshift of optical band gap in ZnO thin films grown by metal-organic chemical-vapor deposition," *Journal of Applied Physics,* vol. 98, no. 1, p. 013505, 2005.
[43] D. Rogers, F. Hosseini Teherani, A. Yasan, K. Minder, P. Kung, and M. Razeghi, "Electroluminescence at 375 nm from a Zn O⁄ Ga N: Mg⁄ c-Al 2 O 3 heterojunction light emitting diode," *Applied physics letters,* vol. 88, no. 14, p. 141918, 2006.

[44] S. Basu and P. Basu, "Nanocrystalline metal oxides for methane sensors: role of noble metals," *Journal of Sensors,* vol. 2009, 2009.
[45] T. Wu, Z. Wang, M. Tian, J. Miao, H. Zhang, and J. Sun, "UV excitation NO2 gas sensor sensitized by ZnO quantum dots at room temperature," *Sensors and Actuators B: Chemical,* vol. 259, pp. 526-531, 2018.
[46] X. Yang *et al.*, "One step synthesis of branched SnO2/ZnO heterostructures and their enhanced gas-sensing properties," *Sensors and Actuators B: Chemical,* vol. 281, pp. 415-423, 2019.
[47] V. Galstyan, E. Comini, I. Kholmanov, G. Faglia, and G. Sberveglieri, "Reduced graphene oxide/ZnO nanocomposite for application in chemical gas sensors," *RSC advances,* vol. 6, no. 41, pp. 34225-34232, 2016.
[48] A. Tabib *et al.*, "Structural and optical properties of Na doped ZnO nanocrystals: application to solar photocatalysis," *Applied Surface Science,* vol. 396, pp. 1528-1538, 2017.
[49] Y. Song, F. Yin, C. Zhang, W. Guo, L. Han, and Y. Yuan, "Three-dimensional ordered mesoporous carbon spheres modified with ultrafine zinc oxide nanoparticles for enhanced microwave absorption properties," *Nano-micro letters,* vol. 13, no. 1, pp. 1-16, 2021.
[50] N. J. Lowe, *Sunscreens: development: evaluation, and regulatory aspects*. CRC press, 1996.
[51] N. M. Bahadur, T. Furusawa, M. Sato, F. Kurayama, I. A. Siddiquey, and N. Suzuki, "Fast and facile synthesis of silica coated silver nanoparticles by microwave irradiation," *Journal of colloid and interface science,* vol. 355, no. 2, pp. 312-320, 2011.
[52] C. Wang, L. Yin, L. Zhang, D. Xiang, and R. Gao, "Metal oxide gas sensors: sensitivity and influencing factors," *sensors,* vol. 10, no. 3, pp. 2088-2106, 2010.
[53] M. Arafat, B. Dinan, S. A. Akbar, and A. Haseeb, "Gas sensors based on one dimensional nanostructured metal-oxides: a review," *Sensors,* vol. 12, no. 6, pp. 7207-7258, 2012.
[54] L. Zhu and W. Zeng, "Room-temperature gas sensing of ZnO-based gas sensor: A review," *Sensors and Actuators A: Physical,* vol. 267, pp. 242-261, 2017.
[55] M. Suchea, S. Christoulakis, K. Moschovis, N. Katsarakis, and G. Kiriakidis, "ZnO transparent thin films for gas sensor applications," *Thin solid films,* vol. 515, no. 2, pp. 551-554, 2006.
[56] N. Chestnoy, T. D. Harris, R. Hull, and L. E. Brus, "Luminescence and photophysics of cadmium sulfide semiconductor clusters: the nature of the emitting electronic state," *The Journal of Physical Chemistry,* vol. 90, no. 15, pp. 3393-3399, 1986.
[57] S. Talam, S. R. Karumuri, and N. Gunnam, "Synthesis, characterization, and spectroscopic properties of ZnO nanoparticles," *International Scholarly Research Notices,* vol. 2012, 2012.
[58] M. H. Huang, Y. Wu, H. Feick, N. Tran, E. Weber, and P. Yang, "Catalytic growth of zinc oxide nanowires by vapor transport," *Advanced materials,* vol. 13, no. 2, pp. 113-116, 2001.
[59] M. Šćepanović, M. Grujić-Brojčin, K. Vojisavljević, S. Bernik, and T. Srećković, "Raman study of structural disorder in ZnO nanopowders," *Journal of Raman Spectroscopy,* vol. 41, no. 9, pp. 914-921, 2010.
[60] F. Güell *et al.*, "Raman and photoluminescence properties of ZnO nanowires grown by a catalyst-free vapor-transport process using ZnO nanoparticle seeds," *physica status solidi (b),* vol. 253, no. 5, pp. 883-888, 2016.
[61] R. Sapkota, P. Duan, T. Kumar, A. Venkataraman, and C. Papadopoulos, "Thin Film Gas Sensors Based on Planetary Ball-Milled Zinc Oxide Nanoinks: Effect of Milling Parameters on Sensing Performance," *Applied Sciences,* vol. 11, no. 20, p. 9676, 2021.
[62] M. Magini, "The role of energy transfer in mechanical alloying powder processing," in *Materials Science Forum*, 1992, vol. 88: Trans Tech Publ, pp. 121-128.
[63] P. Giri, S. Bhattacharyya, D. K. Singh, R. Kesavamoorthy, B. Panigrahi, and K. Nair, "Correlation between microstructure and optical properties of ZnO nanoparticles synthesized by ball milling," *Journal of Applied Physics,* vol. 102, no. 9, p. 093515, 2007.
[64] Y. Tong *et al.*, "Growth and optical properties of ZnO nanostructures by vapor transport process," *Materials chemistry and physics,* vol. 103, no. 1, pp. 190-194, 2007.

[65] J. H. He, C. S. Lao, L. J. Chen, D. Davidovic, and Z. L. Wang, "Large-scale Ni-doped ZnO nanowire arrays and electrical and optical properties," *Journal of the American Chemical Society,* vol. 127, no. 47, pp. 16376-16377, 2005.
[66] X. Wang, J. Zhou, J. Song, J. Liu, N. Xu, and Z. L. Wang, "Piezoelectric field effect transistor and nanoforce sensor based on a single ZnO nanowire," *Nano letters,* vol. 6, no. 12, pp. 2768-2772, 2006.
[67] J. Xu, Q. Pan, and Z. Tian, "Grain size control and gas sensing properties of ZnO gas sensor," *Sensors and Actuators B: Chemical,* vol. 66, no. 1-3, pp. 277-279, 2000.
[68] S. Pilotek and H. Schmidt, "Hydrophobic and Oleophobic Coatings in Sol–Gel Technologies for Glass Producers and Users, Aegerter MA, Mennig M," ed: Eds, 2004.
[69] C. Liewhiran and S. Phanichphant, "Influence of thickness on ethanol sensing characteristics of doctor-bladed thick film from flame-made ZnO nanoparticles," *Sensors,* vol. 7, no. 2, pp. 185-201, 2007.
[70] R. Sapkota, J. Zou, S. Dawka, J. E. Bobak, and C. Papadopoulos, "Multi-functional thin film coatings formed via nanogrinding," *Applied Nanoscience,* vol. 8, no. 6, pp. 1437-1444, 2018.
[71] L. Saikia, D. Bhuyan, M. Saikia, B. Malakar, D. K. Dutta, and P. Sengupta, "Photocatalytic performance of ZnO nanomaterials for self sensitized degradation of malachite green dye under solar light," *Applied Catalysis A: General,* vol. 490, pp. 42-49, 2015.
[72] A. Amutha, S. Amirthapandian, B. Sundaravel, B. Panigrahi, K. Saravanan, and P. Thangadurai, "Low-temperature photoluminescence behaviour of Ag decorated ZnO Nanorods," *Journal of Applied Physics,* vol. 120, no. 20, p. 205104, 2016.
[73] R. Kumar, O. Al-Dossary, G. Kumar, and A. Umar, "Zinc oxide nanostructures for NO 2 gas–sensor applications: A review," *Nano-Micro Letters,* vol. 7, no. 2, pp. 97-120, 2015.
[74] S. Li, J. Wu, Z. M. Wang, and Y. Jiang, *Nanoscale Sensors*. Springer, 2013.
[75] K. K. Varanasi, M. Hsu, N. Bhate, W. Yang, and T. Deng, "Spatial control in the heterogeneous nucleation of water," *Applied Physics Letters,* vol. 95, no. 9, p. 094101, 2009.
[76] M. Jiao, N. Van Duy, N. D. Hoa, N. Van Hieu, K. Hjort, and H. Nguyen, "Comparison of NO 2 gas-sensing properties of three different ZnO nanostructures synthesized by On-Chip low-temperature hydrothermal growth," *Journal of Electronic Materials,* vol. 47, no. 1, pp. 785-793, 2018.
[77] A. B. Khatibani, "Investigation of gas sensing property of zinc oxide thin films deposited by Sol-Gel method: effects of molarity and annealing temperature," *Indian Journal of Physics,* vol. 95, no. 2, pp. 243-252, 2021.
[78] V. S. Bhati *et al.*, "Improved sensitivity with low limit of detection of a hydrogen gas sensor based on rGO-loaded Ni-doped ZnO nanostructures," *ACS applied materials & interfaces,* vol. 10, no. 13, pp. 11116-11124, 2018.
[79] M. Xue, F. Li, Y. Wang, X. Cai, F. Pan, and J. Chen, "Ultralow-limit gas detection in nano-dumbbell polymer sensor via electrospinning," *Nanoscale,* vol. 5, no. 5, pp. 1803-1805, 2013.
[80] V. Demontis *et al.*, "Conductometric sensing with individual InAs nanowires," *Sensors,* vol. 19, no. 13, p. 2994, 2019.
[81] J. Z. Ou *et al.*, "Physisorption-Based Charge Transfer in Two-Dimensional SnS2 for Selective and Reversible NO2 Gas Sensing," *ACS Nano,* vol. 9, no. 10, pp. 10313-10323, 2015/10/27 2015, doi: 10.1021/acsnano.5b04343.
[82] L. Yu *et al.*, "Both oxygen vacancies defects and porosity facilitated NO2 gas sensing response in 2D ZnO nanowalls at room temperature," *Journal of Alloys and Compounds,* vol. 682, pp. 352-356, 2016.
[83] Z. Yuan, R. Li, F. Meng, J. Zhang, K. Zuo, and E. Han, "Approaches to enhancing gas sensing properties: a review," *Sensors,* vol. 19, no. 7, p. 1495, 2019.
[84] D. Vollath, "Nanomaterials an introduction to synthesis, properties and application," *Environmental Engineering and Management Journal,* vol. 7, no. 6, pp. 865-870, 2008.

[85] Y. Kang, F. Yu, L. Zhang, W. Wang, L. Chen, and Y. Li, "Review of ZnO-based nanomaterials in gas sensors," *Solid State Ionics,* vol. 360, p. 115544, 2021.
[86] R. Viswanathan and R. B. Gupta, "Formation of zinc oxide nanoparticles in supercritical water," *The Journal of supercritical fluids,* vol. 27, no. 2, pp. 187-193, 2003.
[87] W. Göpel and U. Lampe, "Influence of defects on the electronic structure of zinc oxide surfaces," *Physical Review B,* vol. 22, no. 12, p. 6447, 1980.
[88] C. A. Aggelopoulos, M. Dimitropoulos, A. Govatsi, L. Sygellou, C. D. Tsakiroglou, and S. N. Yannopoulos, "Influence of the surface-to-bulk defects ratio of ZnO and TiO2 on their UV-mediated photocatalytic activity," *Applied Catalysis B: Environmental,* vol. 205, pp. 292-301, 2017.
[89] A. Tsukazaki, A. Ohtomo, and M. Kawasaki, "High-mobility electronic transport in ZnO thin films," *Applied physics letters,* vol. 88, no. 15, p. 152106, 2006.
[90] P. Wang, T. Dong, C. Jia, and P. Yang, "Ultraselective acetone-gas sensor based ZnO flowers functionalized by Au nanoparticle loading on certain facet," *Sensors and Actuators B: Chemical,* vol. 288, pp. 1-11, 2019.
[91] X. Wang, S. S. Yee, and W. P. Carey, "Transition between neck-controlled and grain-boundary-controlled sensitivity of metal-oxide gas sensors," *Sensors and Actuators B: Chemical,* vol. 25, no. 1-3, pp. 454-457, 1995.
[92] Y. Takahashi, M. Kanamori, A. Kondoh, H. Minoura, and Y. Ohya, "Photoconductivity of ultrathin zinc oxide films," *Japanese Journal of Applied Physics,* vol. 33, no. 12R, p. 6611, 1994.
[93] J.-H. Kim, A. Mirzaei, H. W. Kim, P. Wu, and S. S. Kim, "Design of supersensitive and selective ZnO-nanofiber-based sensors for H2 gas sensing by electron-beam irradiation," *Sensors and Actuators B: Chemical,* vol. 293, pp. 210-223, 2019.
[94] D. Scolfaro, Y. Onofre, M. D. Teodoro, and M. De Godoy, "Atmosphere-dependent photoconductivity of ZnO in the urbach tail," *International Journal of Photoenergy,* vol. 2018, 2018.
[95] B. M. Kulwicki, "Humidity sensors," *Journal of the American Ceramic Society,* vol. 74, no. 4, pp. 697-708, 1991.
[96] S. Ozcan, M. M. Can, and A. Ceylan, "Single step synthesis of nanocrystalline ZnO via wet-milling," *Materials Letters,* vol. 64, no. 22, pp. 2447-2449, 2010.
[97] M. Poloju, N. Jayababu, and M. R. Reddy, "Improved gas sensing performance of Al doped ZnO/CuO nanocomposite based ammonia gas sensor," *Materials Science and Engineering: B,* vol. 227, pp. 61-67, 2018.
[98] D. R. Miller, S. A. Akbar, and P. A. Morris, "Nanoscale metal oxide-based heterojunctions for gas sensing: a review," *Sensors and Actuators B: Chemical,* vol. 204, pp. 250-272, 2014.
[99] Q. Drmosh *et al.*, "UV-activated gold decorated rGO/ZnO heterostructured nanocomposite sensor for efficient room temperature H2 detection," *Sensors and Actuators B: Chemical,* vol. 290, pp. 666-675, 2019.
[100] W.-T. Koo *et al.*, "Chemiresistive hydrogen sensors: fundamentals, recent advances, and challenges," *ACS nano,* vol. 14, no. 11, pp. 14284-14322, 2020.